Evaluation of linkages between climate change and sedimentary biogeochemistry in the glacial/interglacial North Atlantic

Dylan Malynn

A thesis submitted to the faculty of the University of North Carolina at Chapel Hill in partial fulfillment of the requirements for the degree Master of Sciences in the Department of Geological Sciences

Chapel Hill

2011

Approved by:

Advisor: Dr. Stephen Meyers

Reader: Dr. Donna Surge

Reader: Dr. Larry Benninger

© 2011
Dylan Malynn
ALL RIGHTS RESERVED

ABSTRACT

Dylan Malynn

Evaluation of linkages between climate change and

sedimentary biogeochemistry in the glacial/interglacial North Atlantic

(Under the direction of Dr. Stephen Meyers)

Over the past 125,000 years, global climate has varied in lock step with the growth and decay of large continental ice sheets. Concomitant with these large-scale glacial/interglacial climate shifts are marked changes in deep-sea sedimentation in the North Atlantic basin. Warm interglacial climates are generally associated with more $CaCO_3$-rich deep-sea sediments, while cold glacial intervals are typically manifest as more clay-rich intervals. This study examines the impact of these glacial/interglacial sedimentologic changes on benthic (ocean bottom) biogeochemistry, and also investigates potential feedbacks between benthic processes and climate. In addition to documenting the glacial/interglacial response of marine sedimentation in the North Atlantic, with respect to select major, minor and trace elements that can be used to reconstruct changes in lithogenous, biogenic and authigenic processes, this work addresses a number of key biogeochemical interactions that centrally involve iron, which is plentiful in the clay-rich glacial sediments, but scarce in the interglacial sediments.

TABLE OF CONTENTS

LIST OF TABLES

LIST OF FIGURES

1. INTRODUCTION

The Late-Pleistocene is characterized by pronounced climate variability (Figure 1A) that exhibits a clear synchronization with the carbon cycle (Figure 1B) and large-scale changes in Northern Hemisphere glaciation (Figure 1C) (e.g. Clark et al., 1999, Seigenthaler et al., 2005). While the details of these climatic, oceanographic and biogeochemical linkages are a source of ongoing debate (e.g. Broecker, 1982, Lynch-Stieglitz et al., 2007, Brovkin et al., 2007), comparatively little attention has been given to the glacial/interglacial response of North Atlantic benthic biogeochemistry (diagenesis), and the potential role of benthic processes as a feedback on climate change (however, see Berger, 1982, Berger and Killingley, Tamburini et al., 2002, Tamburini et al., 2003a,b). Pertinent to this issue, the growth and decay of large-scale continental ice sheets (Hays et al., 1976) had a profound impact on the character of deep-sea sedimentation in the North Atlantic Basin (Figure 1E, Figure 2). Basin-wide mapping of wt.% $CaCO_3$ in North Atlantic Ocean sediments indicates that biogenic carbonate deposition is dominant during warm interglacial periods, whereas glacial times are manifest as clay-rich intervals (Balsam and McCoy, 1987). These systematic variations in sedimentation are the consequence of eustatic sea level fall driven by ice sheet growth, resulting in the redistribution of exposed clay-rich continental shelf sediments to the deep-sea (Ruddiman and Bowles, 1976, Balsam and Huesser, 1976, Balsam, 1981). This

process was likely augmented by a decrease in carbonate saturation in the North Atlantic Ocean during the glacial times, at least in the deeper portions of the water column (Thunell, 1982).

In this study, I seek to evaluate the impact of the glacial/interglacial sedimentologic shifts (e.g. clay versus calcium carbonate content) on benthic biogeochemistry, diagenesis, and potential feedbacks with climate change. Special focus is given to a number of key biogeochemical processes that centrally involve iron, which is plentiful in glacial clay-rich sediments, but is extremely scarce in interglacial sediments. The specific objectives of this work include:

Objective 1: To document the glacial/interglacial response of marine sedimentation in the North Atlantic, with respect to select major, minor and trace elements that can be used to reconstruct changes in lithogenous, biogenic and authigenic processes. *This objective will be achieved via XRF core scanning, a technique that allows the generation of continuous high-resolution geochemical profiles for qualitative evaluation of geochemical variability. Factor analysis will be utilized to assist in the attribution of particular elements to lithogenous, biogenic, and authigenic sources.*

Objective 2: To test the hypothesis that the dominant glacial/interglacial sedimentologic shifts (clay versus calcium carbonate content) are also paralleled by changes in redox state and biogeochemical remineralization processes within the sediments. *This will be accomplished by integrating*

relevant XRF core-scanning data (redox sensitive elements) with an analysis of phosphorous speciation (the SEDEX method; Ruttenberg, 1992), which is particularly responsive to changes in redox state.

Objective 3: To test the hypothesis that enhanced iron delivery during glacial times diminished the regeneration of phosphorous to the water column by adsorption onto iron oxyhydroxides near the sediment-water interface, potentially impacting nutrient availability for primary productivity. *This will be accomplished by evaluation of changes in the amount of iron oxyhydroxide-sorbed phosphorous (Ruttenberg, 1992) through the glacial/interglacial cycles.*

I focus my investigation on a 228 centimeter long gravity core collected from the Rockall Trough/Rockall Plateau region of the North Atlantic (EWR-2101; Figure 3), located between Scotland and Iceland. The core was recovered from 1150 meters water depth on the Rockall Plateau, a relatively shallow area that is flanked to the southeast by the Rockall Trough (Figure 3). As will be demonstrated in the present study, the sheltered depositional environment at this location permitted the accumulation of a surprisingly long record (spanning at least marine isotope stages 1-5, over 125,000 years) across the 228 centimeters of core. Of critical importance to this investigation, the core is in an ideal location to capture the pronounced changes in wt.% $CaCO_3$ that have been documented in previous studies (Balsam and McCoy, 1987; Figure 2). Also of note, paleoclimate/paleoceanographic investigation of the Rockall Plateau region has received relatively little attention in previous

work, and my analyses provide a complement to well-developed records from the Rockall Trough (e.g. Bond et al., 2001, Tamburini et al., 2003a; Figure 3).

This thesis is organized as follows. I begin with a background review of the late-Pleistocene paleoclimate context of the study (*Section 2.1*), followed by a discussion of the multiple sources of geochemical components (lithogenous, biogenic, authigenic) to marine sediments (*Section 2.2*), and finally a discussion of the phosphorous cycle in marine sediments (*Section 2.3*). These topics provide the foundation for my investigations of the EWR 2101 core. Following a detailed discussion of the geochemical methods used in this study (*Section 3*), I then develop a chronostratigraphy for the EWR 2101 core (*Section 4.1*), via correlation of a new high-resolution wt.% $CaCO_3$ record (derived from XRF scanning data, calibrated to coulometric wt.% $CaCO_3$ data) to a benthic foraminifera oxygen isotope stack (Lisiecki and Raymo, 2005). This chronostratigraphic approach is based on previous studies that demonstrate the covariation of oxygen isotopic variability and the wt.% $CaCO_3$ content of North Atlantic sediments (Ruddiman and McIntyre, 1981, Ruddiman and McIntyre 1984, Ruddiman et al., 1989; compare Figure 1C and 1E). We supplement this chronostratigraphic approach with two radiocarbon dates that were acquired for the present study.

In *Section 4.2*, I provide a more comprehensive analysis of the wide range of XRF core scanning elements acquired for EWR 2101, assisted by application of factor analysis to identify lithogenous, biogenic and authigenic contributions. The phosphorous speciation results for EWR 2101 are introduced in *Section 4.3*. Finally,

in *Section 4.4*, I integrate the above data sets to specifically address the three main objectives outlined above, and then conclude with a summary of the key findings of this thesis (*Section 5*).

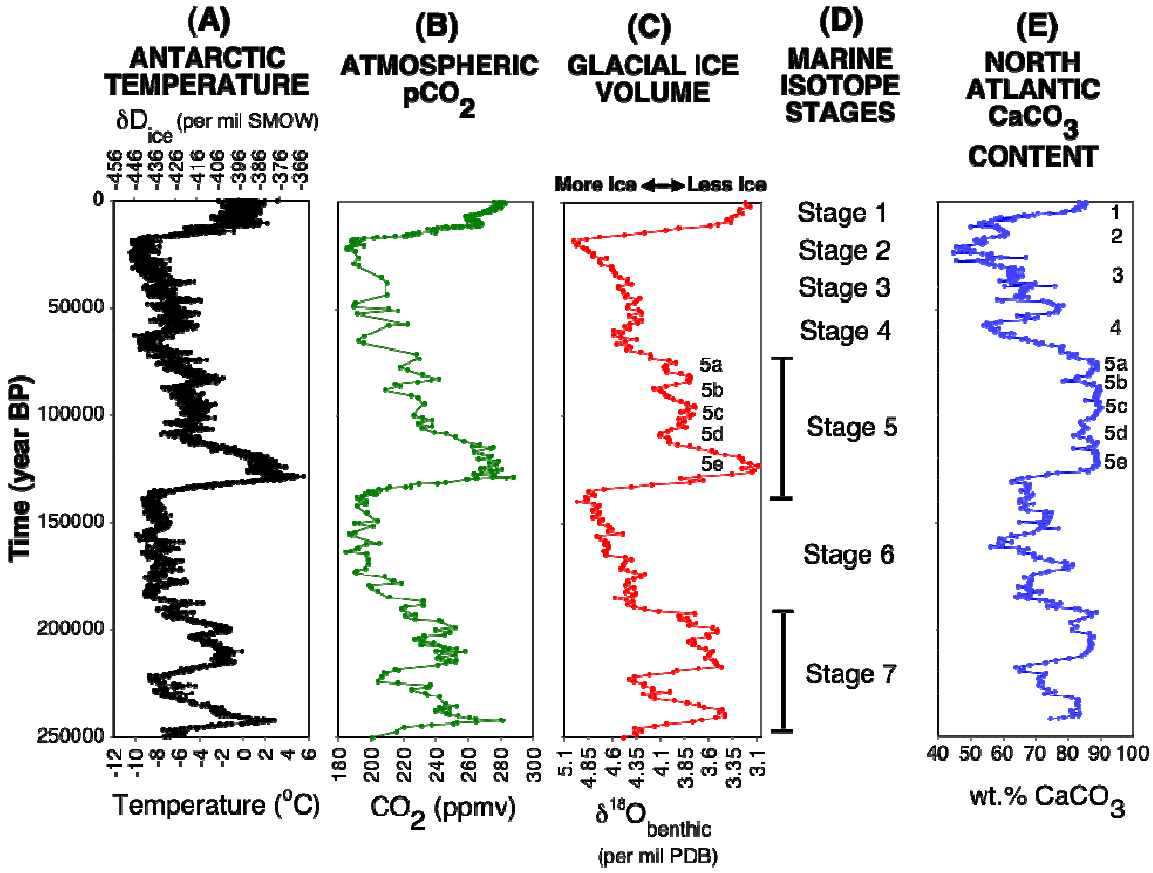

FIGURE 1. Paleoclimate Context for the North Atlantic Ocean: (A) Antarctic temperature reconstructed from ice core using deuterium isotopic data from ice (Jouzel et al., 2007). (B) Atmospheric carbon dioxide concentration from gas bubble in Antarctic ice cores (Jouzel et al., 2007). (C) Benthic foraminifera oxygen isotope stack of Lisiecki and Raymo (2004), a measure of glacial ice volume. (D) The Marine isotope stages (Emiliani, 1955). (E) The concentration of calcium carbonate in North Atlantic sediments deposited at 41.002°N, 32.957°W (Ruddiman et al., 1989).

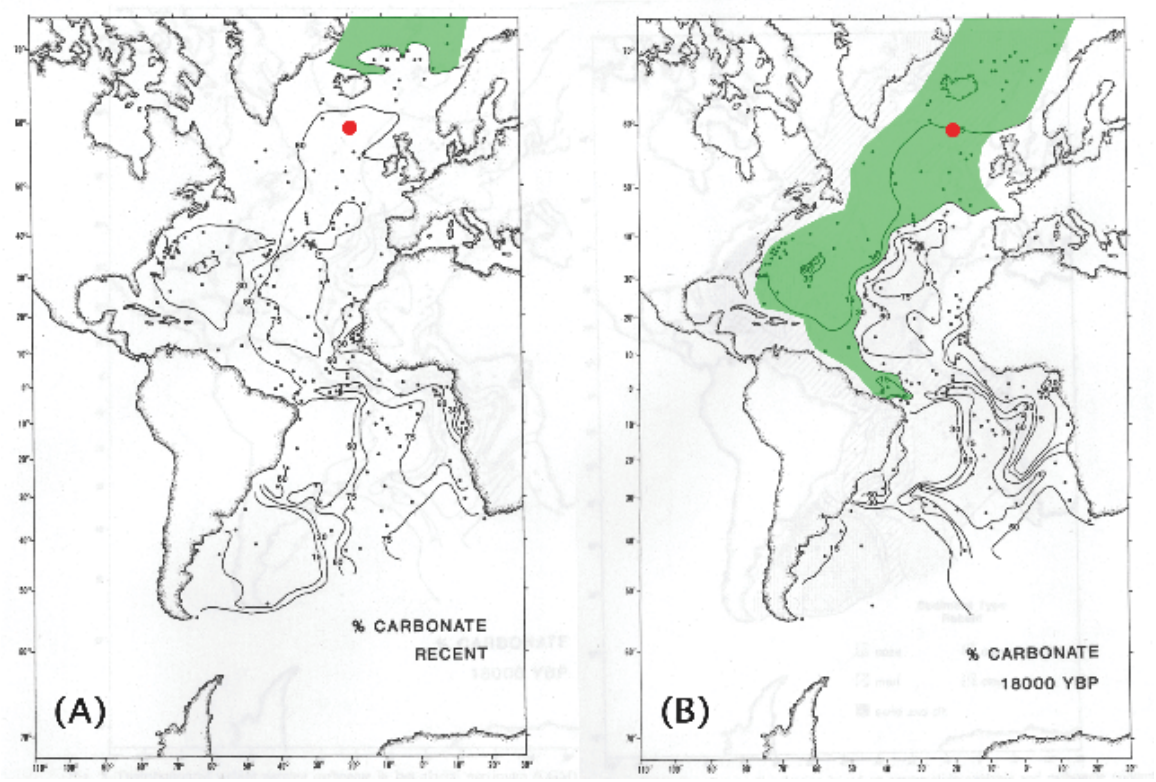

FIGURE 2. Calcium carbonate content of North Atlantic sediments during glacial/interglacial cycles: A comparison of weight percent calcium carbonate depositional patterns in the North Atlantic during the peak glacial (~18,000 years ago; Fig 2B) and present (Fig 2A). The light green area indicates clay-rich, carbonate poor sediments (< 30 wt. % $CaCO_3$), and the red circle identifies the location of the EWR2101 gravity core analyzed in this study. Note that most of the North Atlantic ocean is characterized by pronounced changes in wt.% $CaCO_3$ between glacial and interglacial times, which should be captured by core EWR 2101. Figure modified from Balsam and McCoy, 1987.

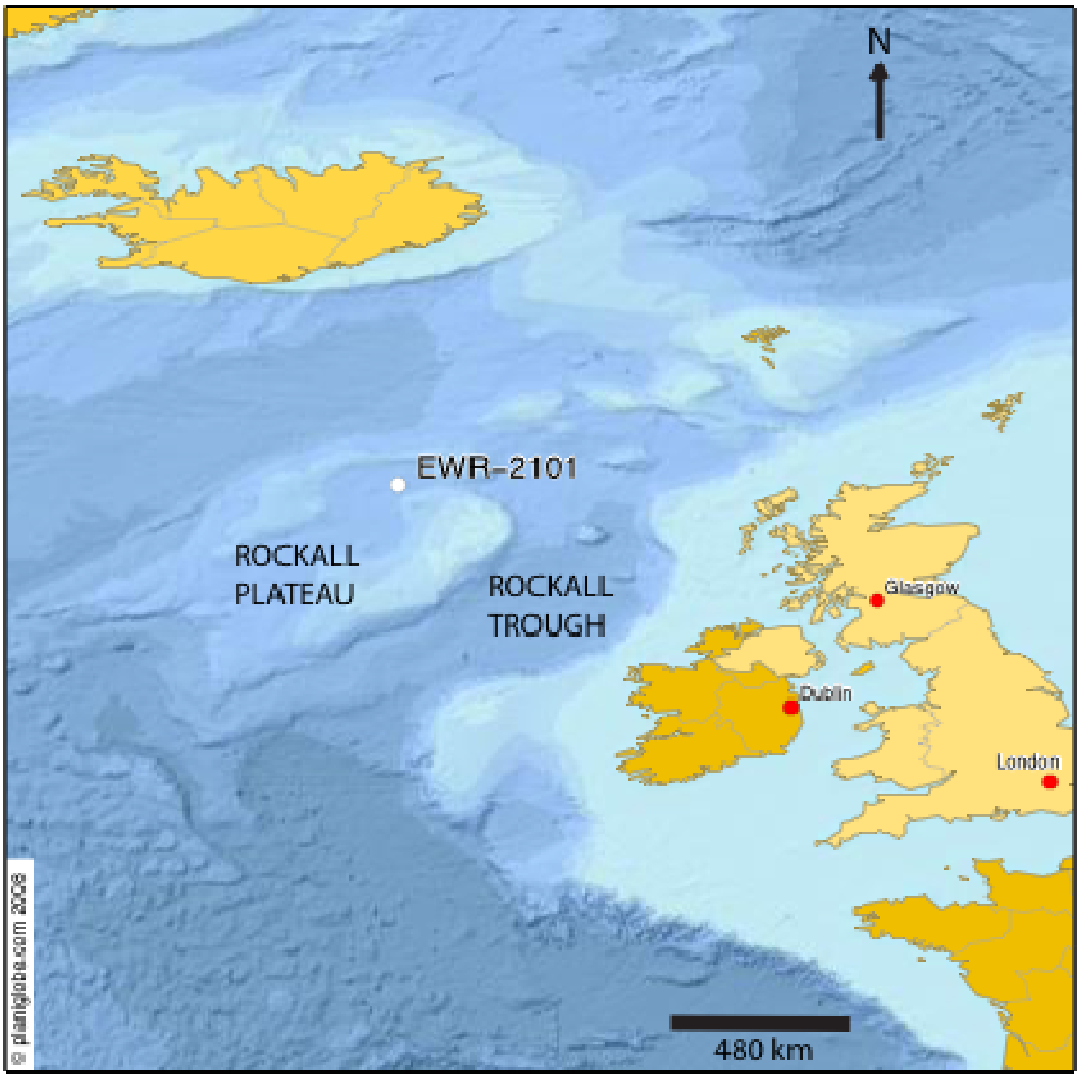

FIGURE 3. EWR-2101 location map: (generated from www.planiglobe.com).

Location of sample core (EWR 2101) in the Rockall Region, North Atlantic

2.1. BACKGROUND: Late-Pleistocene Paleoclimate Context

Rapid changes in polar ice volume, temperature, formation of deep water and the global carbon cycle punctuate the Late Pleistocene and are a major focus of on-going paleoclimate research (Figure 1). The climate system fluctuates between glacial and interglacial states creating a "sawtooth" pattern in the climate record, and is likely influenced by orbital-insolation changes (Ganapolski and Rahmstorf, 2000). Evidence suggests (Keigwin and Jones, 1994, Jaccard et al., 2005, Dansgaard et al., 1993) that the impact of climate variability during this period is widespread geographically and throughout various geosystems, including a coupled response in the atmosphere-ocean-sea ice system (Alley et al., 2003).

Density driven fluctuation in the rate of thermohaline circulation (THC) is the most viable explanation for the abrupt, pervasive variability displayed in indicators of both air and ocean temperatures. THC provides an extremely efficient path for heat flow from tropical to polar regions and is largely responsible for climate moderation in the mid-lattitudes (Ganachaud and Wunsch, 2000). Input of fresh water, via sea ice melting or meltwater runoff, can create a strong density stratification in key regions of deep water formation, which acts as a barrier to vertical mixing. This rapid shut-down of THC can cause abrupt cooling in both the ocean and atmosphere in polar regions and warming in the tropics due to decreased heat export (Broecker, 1998).

The impact of changes in THC is pervasive both geographically and throughout the global climate system and can be observed in a multitude of proxy data. The LRO4 benthic foraminfera stack provides an extremely detailed record of

these fluctuations in salinity, temperature and glacial ice volume that are likely driven by circulation changes. By coupling this data with carbonate records from the North Atlantic (Ruddiman et al., 1989) and EPICA Dome C ice core data (Antarctica), it is evident that the influence of short-term (1-100kyr) climate change is widespread geographically and has a profound impact on global temperatures, glacial ice volume, biological productivity, the global carbon cycle and marine sedimentation.

2.2. BACKGROUND: Lithogenous, Biogenic and Authigenic Contributions to Marine Sediments

Fine-grained marine sediments are an aggregate of terrigenous, biogenic and authigenic fluxes (e.g. Potter et al., 1980, Gorsline, 1984, Arthur and Sageman 1994; Figure 4). The terrigenous component of the sediments is largely derived from volcanism and the weathering of continental crust and is delivered to marine basins by fluvial and eolian transport. Terrestrial and marine biogenic material is supplied to the sediments in the form of organic matter and skeletal remains produced by photosynthetic, chemosynthetic and heterotrophic processes. The authigenic fraction precipitates primarily in the sediment pore waters as a result of Eh-pH driven reactions.

A common approach to resolving the contribution of each pool to the sediments is utilization of elemental proxies and ratios. Under normal weathering conditions, the most reliable proxies for direct input from crustal weathering are Si (detrital quartz), Al and K from clays (Pratt, 1984), and Ti and Zr (zircon, rutile,

sphene, titanite; Arthur et al., 1985). Iron is not as reliable as a pure indicator of terrigenous input due to its involvement in several key redox reactions, including precipitation as authigenic ferric-oxyhydroxides or as pyrite. However, due to its strong covariance with the climate signal over the past 125kyr in the North Atlantic, it is reasonable to assume that it is largely representative of the detrital flux to the sediments.

Although calcium is delivered to marine sediments from detrital sources (e.g., clay minerals), the vast majority of the signal in pelagic settings occurs in the form of biogenic $CaCO_3$. Due to the geometry of the study-site basin and the correlation between XRF Ca counts and coulometrically derived wt. % carbonate, we infer that the majority of the Ca signal is associated with biogenic carbonate sources (e.g., foraminifera tests). Due to its propensity for substitution for Ca in the lattice of $CaCO_3$ minerals, Sr also commonly reflects the input of carbonate to the system.

Previous studies (Mayer et al., 1981. Ziegler et al., 2008) indicate that bromine is a useful indicator of input of marine organic matter to the sediments (in the form of macroalgae). However, lack of a definitive endmember Br:OC value of purely marine algae challenges the use of Br as a quantitative indicator of marine OM flux to the sediments. Barium concentration in the sediments is also useful as an indicator of paleoproductivity (e.g. Schmitz, 1987, Shimmield et al., 1988, Paytan and Kastner, 1996), however the preservation rate is approximately 30% in oxic settings. Regeneration in the water column also complicates interpretation, however Ba (particularly if normalized to the detrital flux) remains potentially useful as a rough indicator of paleoproductivity.

Manganese, vanadium, chromium and sulfur distributions provide insight to sediment redox cycling during early diagenesis. During organic matter remineralization, MnO_2 is utilized as a terminal electron acceptor in suboxic conditions. This process, coupled with upward mobility and re-precipitation in the oxic zone, has a focusing effect in marine sediments causing the Mn profile to largely correlate with reactive Fe (Froelich et al., 1978).

Vanadium prevails largely in well-oxygenated waters as the vanadate oxoanion $H_xVO_4^{-3+x}$, and shows a strong affinity to adsorbtion on the surface of ferric-oxyhydroxides and complexation with organic ligands (Baes and Mesmer, 1976, Wehrli and Stumm, 1988). It is also stable in mildly reducing conditions as VO^{+2}, but is largely replaced by chromate on sorbtion sites under more acidic conditions.

Chromium exists in oxic environments as $H_xCrO_4^{-2+x}$, however is quickly reduced to Cr(III) in the presence of reduced Fe or S. As a result, Cr/V is a useful indicator of reducing conditions as the reduced form of chromium sorbs more strongly to oxyhydroxides than vanadium (Richard and Bourg, 1991).

Under anoxic conditions, sulfate (SO_4^{-2}) is converted to H_2S via organic matter remineralization. The sulfide produced by this reaction combines with sedimentary iron to form the authigenic mineral pyrite (FeS_2), which, in high concentrations, indicates the presence of substantial hydrogen sulfide concentrations in the water column and/or pore waters (Goldhaber and Kaplan, 1974, Berner, 1984). As a result, sulfur concentration is useful as an indicator of past anoxia, however interpretation is complicated by incomplete preservation due to

later bioturbation and the input of oxygen (Goldhaber and Kaplan, 1974, Berner, 1984).

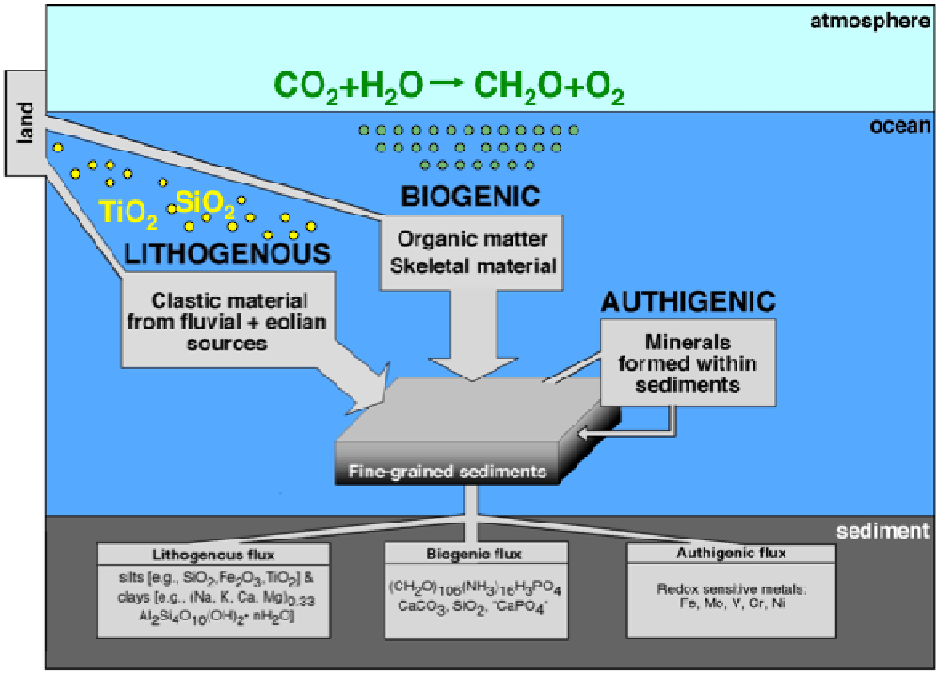

FIGURE 4. Lithogenous, biogenic and authigenic sedimentary inputs: Illustration of potential geochemical contributions to marine sediments, divided into three broad categories: lithogenous, biogenic and authigenic. Figure modified from Sageman and Lyons (2003).

2.3. BACKGROUND: The Phosphorous Cycle

The global phosphorous cycle is comprised of four primary components: weathering and erosion of phosphorous contained in rocks and minerals, fluvial transport to the oceans, utilization by organisms, and incorporation in sediments. Tectonic processes may complete the cycle by returning the phosphorous-bearing sediments to the surface (Ruttenberg, 1993). The primary initial source of reactive phosphorous to the oceans is fluvial input, however return flux from remineralization of organic matter plays a crucial role in the ultimate availability for biological productivity. As a result, a complete understanding of phosphorous-cycling during burial and diagenesis is central to resolving the interaction between carbon, phosphorous and climate on geologic timescales.

The distribution of bioavailable (reactive) phosphorous in the oceans and in marine sediments is intimately linked with the global carbon cycle because it is an essential nutrient for life. The commonly-accepted Redfield Ratio (Redfield, 1934) for marine organic matter is 106C:16N:1P, which suggests that phosphorous acts as a limiting nutrient in many marine systems. Remineralization of organic matter is a key mechanism for delivery of dissolved reactive phosphorous to the water column. Diffusive fluxes from sediment pore water return much of the phosphorous to the water column, however a portion is lost to deep burial due to incomplete oxidiation of organic material. In addition, iron oxyhydroxides can trap remineralized phosphorous via sorption on their surfaces (Krom and Berner, 1980), impacting

nutrient availability for primary production. These factors represent fundamental linkages between iron, phosphorous, and the global carbon cycle.

Vertical mixing in the oceans plays a fundamental role in both the phosphorous and global carbon cycles. Biological activity in marine surface water relies heavily on upwelling of nutrient-rich bottom waters. Decreased vertical mixing can cause coincident increases in anoxia and the concentration of dissolved phosphorous in the deep ocean.

A major focus of investigation has been the cycling of Fe-bearing minerals and the impact they have on the return of PO_4 to the water column. During organic matter remineralization, Fe^{3+} acts as an electron receptor after exhaustion of oxygen, nitrate and manganese. This process builds up water-soluble Fe^{2+} in the porewaters, creating a concentration gradient and producing a flux toward the water column. Upon encountering the oxic/anoxic boundary layer, the dissolved iron is oxidized, forming highly insoluble ferric oxy-hydroxides that can adsorb phosphate. Subsequent burial of sediment and diagenesis completes the cycle by moving the Fe-bearing minerals back down into reducing conditions. (Burdige, 2006)

Delivery of reactive iron and oxygenation state of bottom waters plays a vital role in early-diagenesis of phosphorous, in particular the ability of sediments to act as a long-term sink for dissolved phosphate. Phases that effectively remove phosphorous from the water column include carbonate fluorapatite, oxide-bound P and organic P, in contrast to detrital apatite, a form that is not involved in scavenging. Delivery of phosphorous to the sediments occurs in all of the

aforementioned forms, but is only exchanged between the sorbed, organic, dissolved and authigentic phases (Ruttenberg, 1992) (Figure 5). Of particular note is the movement of phosphorous from organic (via remineralization) and sorbed (via reduction) states to the dissolved pool during burial. These processes create a gradient of aqueous phosphate from reducing zones in the sediment toward the oxic zone and water column. Upon reaching the oxic layer, dissolved P shows an affinity for sorbtion on the surfaces of ferric-oxyhydroxides, which act as a trap preventing liberation to the overlying water column. Upon subsequent overlayering of sediments and bioturbation, the sorbed P again reaches reducing conditions where it is released from mineral surfaces back to the dissolved pool. This process effectively sustains elevated levels of dissolved phosphorous in pore waters and allows for development of authigenic fluorapatite, which acts as a long-term sink for phosphorous.

In addition to playing a fundamental role in phosphorous diagenesis, iron has important consequences for the global carbon cycle. It is established as an essential micronutrient that can limit organic matter production and decrease the amount of CO_2 expelled for a given amount of organic matter consumed by heterotrophic bacteria (Tortell et al., 1996). This is potentially a strong positive feedback to global cooling.

Beyond its impact on marine primary production, iron can potentially play a central role in organic matter burial and the redox state of marine sediments, particularly through the buffering of sulfide via iron sulfidization. This process can potentially expand the oxic-zone in marine sediments, promoting

bioirrigation/bioturbation, phosphorous cycling and the remineralization of organic matter via aerobic respiration by increasing oxygen-exposure time (Meyers, 2007). Iron oxyhydroxides, which are the most active form of iron in sulfide buffering (Canfield et al., 1992), are also the most efficient at trapping dissolved phosphate (Ruttenberg, 1993). As a result, strongly reducing conditions and high concentrations of hydrogen sulfide may inhibit the ability of sediments to adsorb phosphorous causing additional P enrichment in deep water.

During periods of high reactive-iron flux to the sediments, the expansion of the oxic zone along with the adsorbtion of phosphorous on the surfaces of iron-oxyhydoxides minerals presents an extremely efficient sink for both phosphorous and reactive iron. This process represents a potential link between phosphorous, sulfur, iron and the global carbon cycle.

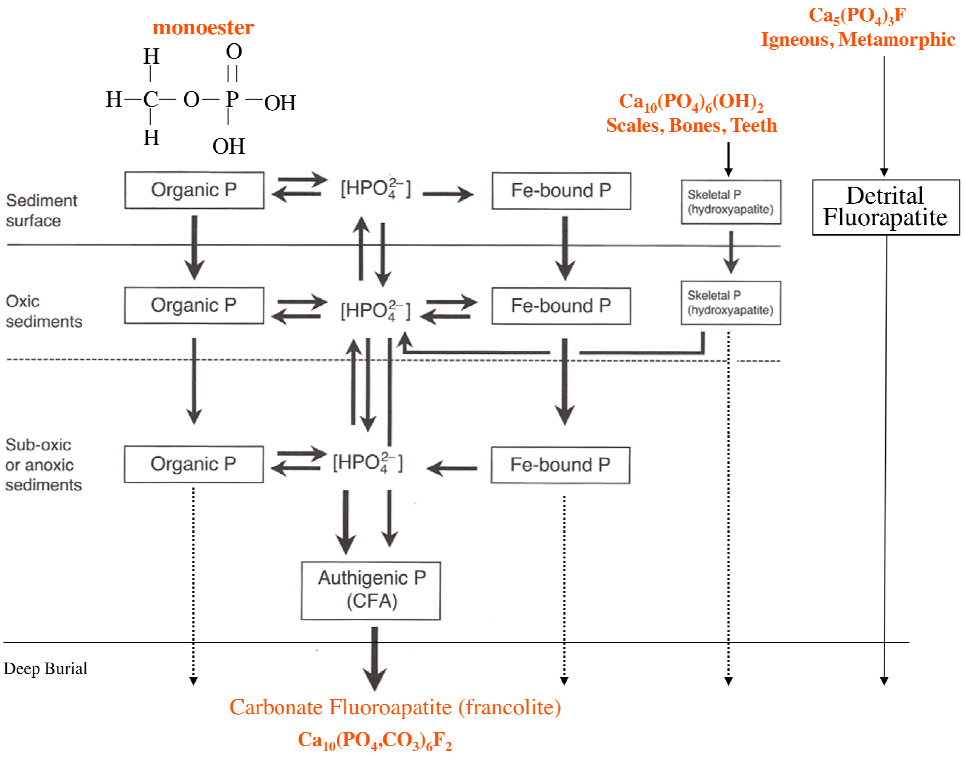

FIGURE 5. Phosphorous Diagenesis: Diagram illustrating the different phosphorous contributions to marine sediments, and the multiple transformations involved in phosphorous diagenesis (Figure modified from Burdige, 2006).

TABLE 1. Methods

AMS Dating	**Absolute Age Control**
XRF Scanning	**Rapid, Non-destructive, Relative Bulk-Geochemistry, Chronology**
Coulometry	**%TOC, %IC**
SEDEX	**Oxide-Sorbed P, P_{auth}, $P_{detrital}$**
UV-Visible Spectrophotometry	**Colorimetric Analysis of P_{auth} and $P_{detrital}$ Samples**
ICP-MS	**Analysis of Oxide-Sorbed P Samples**

3.1 METHODS: Core Acquisition and Preparation

Core samples were initially collected by Surface Geochemical Services AS in 1996. The expedition was funded by the Exxon Corporation in an attempt to assess potential hydrocarbon reservoirs near the Hebrides, Rockall Trough and Rockall Bank. The majority of the sampling was done via gravity core. Unsplit cores were donated to the UNC Department of Geological Sciences in 2005. Cores were split during the summer of 2006, immediately scraped perpendicular to the core-axis to ensure a flat surface for XRF-scanning, packaged in airtight plastic and refrigerated. Samples for wet geochemical analysis were carefully removed at 3cm intervals and placed into air-tight vials. All samples for wet-chemical analysis were oven-dried at 50 degrees-C and homogenized with an agate mortar and pestle.

The cores consist of calcareous ooze layers and dense silt and clay layers. The contact between layers is typically sharp, however gradational transitions are present in some areas. Carbonate-rich sections range from fine to medium-grained

sand and are generally white, while terrigenously-derived layers are consistently clay to silt and range in color from dark brown to green.

3.2 METHODS: X-Ray Fluorescence Core-Scanning

Non-destructive bulk geochemical analysis was performed on the cores using an Avaatech XRF core scanner, which utilizes a 100W X-ray source with a rhodium anode and 125 μm thick beryllium window. The X-ray source generates a beam, which passes through a 99.6% purity He-flushed measurement chamber en route to the core surface. The resulting X-ray fluorescence of the sample was measured by a Si PIN-diode detector, and assigned to element-specific energy windows by a Canberra DSA-1000 digital signal processor. Cores were scanned at 5kV, 10kV, 30kV and 50kV over the entire detection spectrum (Al-U) and in succession to ensure consistent positioning for scans of all energy. Each interval of 1cm was scanned at all given energy levels for sixty seconds.

3.3 METHODS: Wet Chemistry Determination of Organic Carbon, Inorganic Carbon, and Phosphorous

Wt.% $CaCO_3$ and wt.% organic carbon were determined by a two-phase coulometric process consisting of an acidification step and a combustion step. The inorganic step involved treatment with heated 2M hydrochloric acid. The evolved CO_2 was shuttled into the coulometer where the CO_2 was electrochemically titrated. The determination of total carbon (inorganic + organic carbon) began by oxidization

and conversion of all carbon to CO_2 via combustion. Organic carbon was determined by simple subtraction of inorganic carbon from total carbon.

The SEDEX method (Ruttenberg, 1992; Figure 6) was utilized to evaluate different phosphorous contributions to the sediment. The technique is an operationally-defined sequential extraction procedure designed to exploit differences in the reactivity of phosphorous phases to determine their fraction. The method applied for this study was a slight variation of that detailed in Ruttenberg, 1992. The main deviation from the original method was the combination of steps I and II due to the similarity of their behavior in a natural setting. As a result, this study separated the phosphorous content of sediment samples into four pools; loosely-sorbed and oxide-sorbed P (primarily on Fe and Mn-oxyhydroxides), authigenic carbonate fluorapatite, detrital P (in the form of igneous and metamorphic apatite) and organic P.

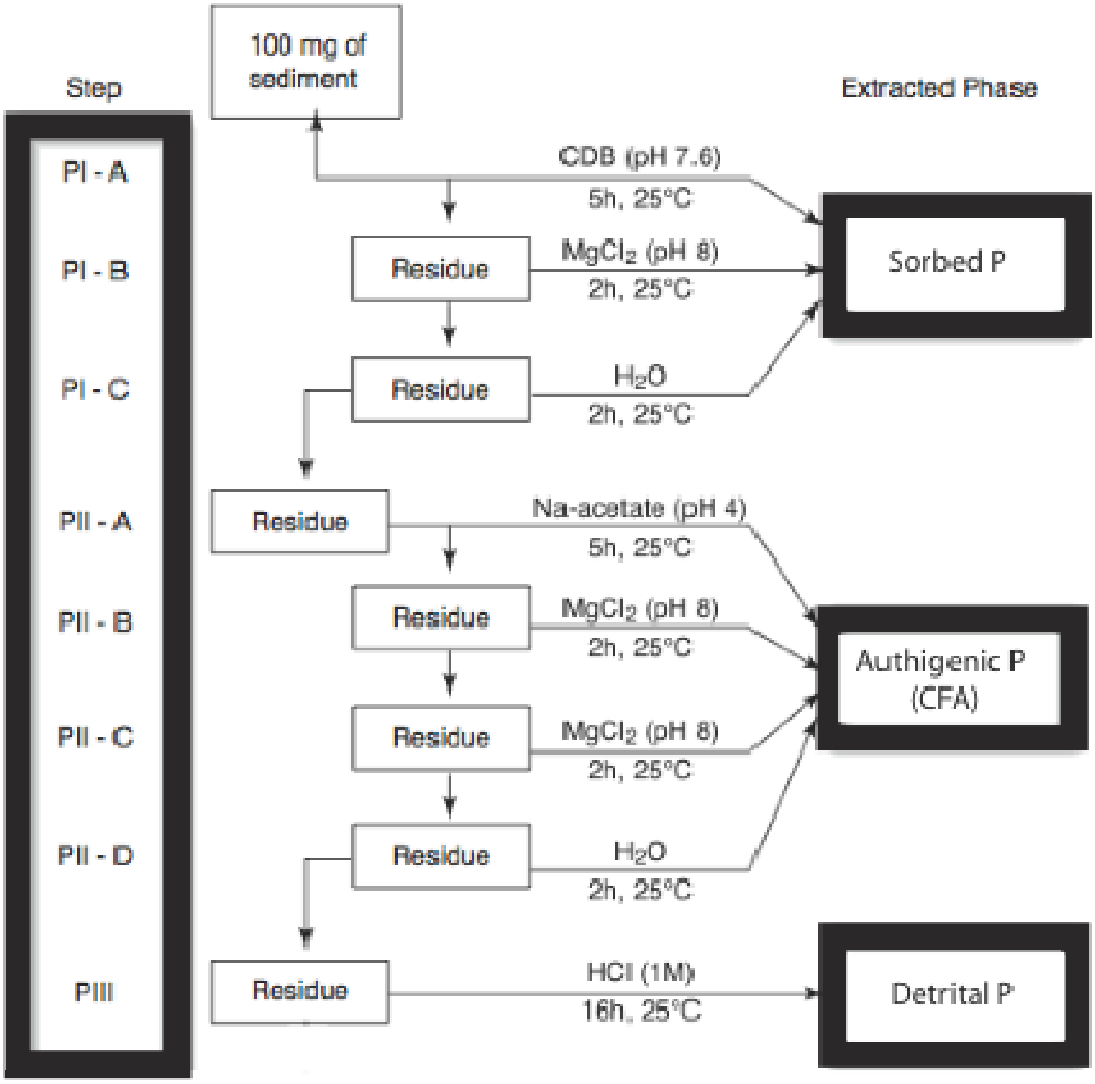

FIGURE 6. Flow diagram for SEDEX procedure: Modified from Tamburini, 2001

The initial step involved measuring 0.1g +/- .001g of sediment and treating it in a polypropylene centrifuge tube with 10ml of 0.3M Na_3-citrate, 1.0M $NaCaCO_3$ solution buffered to 7.6 pH. 0.26g of Na-dithionite was added to act as a reducing agent and the solution was allowed to react for 8 hrs on a shaker table. On completion of the extraction, supernatants were separated into scintillation vials.

The initial extraction was followed by successive rinses in 8.0 pH buffered $MgCl_2$ and milli-Q water rinses. The supernatants were separated and pooled with the initial extract to be measured via ICP-MS, representing the sorbed phosphorous fraction.

Upon completion of the first extraction, 10 ml of 1M Na-acetate buffered to pH 4 with acetic acid was added in order to leach authigenic phosphorous. This reaction proceeded for 6 hrs with interspersed periods of gas release, which was necessary in order to prevent seals from bursting due to overpressure. Upon completion, supernatants were removed and the remaining sample was rinsed twice with $MgCl_2$ solution and once with Milli-Q water. Supernatants from all stages were immediately separated and acidified to a pH of 1 with hydrochloric acid.

The third phase involved a 6 hr extraction of detrial P in 10 ml of 1M hydrochloric acid, followed by successive rinsing twice with $MgCl_2$ and once with milli-Q water. Again, supernatants were removed and acidified to a pH of 1 with hydrochloric acid.

Extraction of organic P began by transferring the remaining sediment samples into borosilicate vials with milli-Q water. Vials were covered in Al-foil and placed in an oven heated to 110 degrees-C until more than half the fluid was removed. 0.5 ml of 50% w/v $Mg(NO_3)_2$ was added, homogenized with the sample and allowed to dry completely in the oven. Once dry, the samples were baked for 2 hrs at 550 degrees-C in order remove the P from organic structures. The remaining residue was soaked in 5 ml of 1M HCl and transferred back to centrifuge tubes. An additional 5 ml of 1M HCl was then added, and allowed to react for 16 hrs on a

shaker table to ensure complete extraction. Supernatants were filtered with 0.45 micron filters and placed in scintillation vials.

The detrital phosphorous and authigenic phosphorous fractions were measured via UV-visible spectrophotometer. The standard two-solution phosphomolybdate blue was followed, which involved treatment of orthophosphates with an acidified molybdate reagent and potassium antimonyl tartrate to form phosphomolybdic acid. This complex was mildly reduced by ascorbic acid to form the molybdenum blue compound. The original phosphate content of the solution was determined by measuring the resulting blue color at 880nm on a UV-visible spectrophotometer and by calibrating the results to standard phosphate solutions.

3.4 METHODS: Accelerator Mass Spectrometer ^{14}C Dating

Age-control is provided by two Accelerator Mass Spectrometer radiocarbon dating, determined from hand-selected planktonic foraminfers. The analyses were performed at the National Ocean Sciences Accelerator Mass Spectrometer Facility (Woods Hole Oceanographic Institution). A reservoir correction of 400 years was applied and the AMS ages were calibrated according to Fairbanks, et al. 2005. All ages are given in years before 1950.

4.1 RESULTS: EWR 2101 Chronostratigraphy

The chronostratigraphy for EWR 2101 primarily relies upon a strong covariation between benthic foraminifera $\delta^{18}O$ (Lisiecki and Raymo, 2005) and wt.% $CaCO_3$ content, as previously documented for North Atlantic sediments (Figure 1; Ruddiman, 1989). Application of this approach requires the development of an accurate high-resolution wt.% $CaCO_3$ record for EWR 2101. We construct an appropriate record via XRF-core scanning, followed by calibration of the XRF results using coulometrically determined wt.% $CaCO_3$. The calibrated wt.% $CaCO_{3\text{-}XRF}$ is then matched to the orbitally-tuned LR04 benthic foraminifera stack, which is the current standard for Plio-Pleistocene oxygen isotope stratigraphy (Lisiecki and Raymo, 2005).

The XRF core scanning data for calcium (Ca_{XRF}) is displayed in Figure 7A, and was acquired continuously at 1 cm resolution. One approach to developing a high-resolution wt.% $CaCO_{3\text{-}XRF}$ record is to estimate carbonate content directly from Ca_{XRF}. However, an important finding of the present study is that the fidelity of the wt.% $CaCO_{3\text{-}XRF}$ reconstruction can be improved by first normalizing Ca_{XRF} by Fe_{XRF} (Figure 7C), followed by a logarithmic transform (Figure 7D). In fact, this approach has a strong foundation in theory. First, normalization of Ca_{XRF} by Fe_{XRF} will suppress changes in Ca_{XRF} that are associated with lithogenic Ca, and also will dampen minor variability in Ca_{XRF} that is associated with changes in bulk density across the core. Furthermore, a logarithmic transformation is appropriate because the calcium fluorescence emitted from the EWR 2101 sediments is nonlinearly related to the true calcium concentration, due to matrix effects with other elements.

The calibration of $Log_{10}(Ca_{XRF}/Fe_{XRF})$ to wt.% $CaCO_3$ is illustrated in Figure 8, indicating that 87.25% of the variance in wt.% $CaCO_3$ can be accounted for in the calibration (p-value= 4.796e-14; compare this to 82.05% for the Ca_{XRF} data alone, with a p-value of 5.927e-12). The remaining 12.75% that cannot be accounted for is potentially attributable to bulk density and/or lithogenic-Ca variability that is not accommodated in our approach. More likely, however, this discrepancy is due to the fact that we are comparing results from geochemical methods that measure somewhat different substrates. While the XRF scanning technique measures fluorescence within millimeters of the sediment surface, the coulometric wt.% $CaCO_3$ is based on the digestion of a homogenized sample that is roughly 1 cm^3 in size.

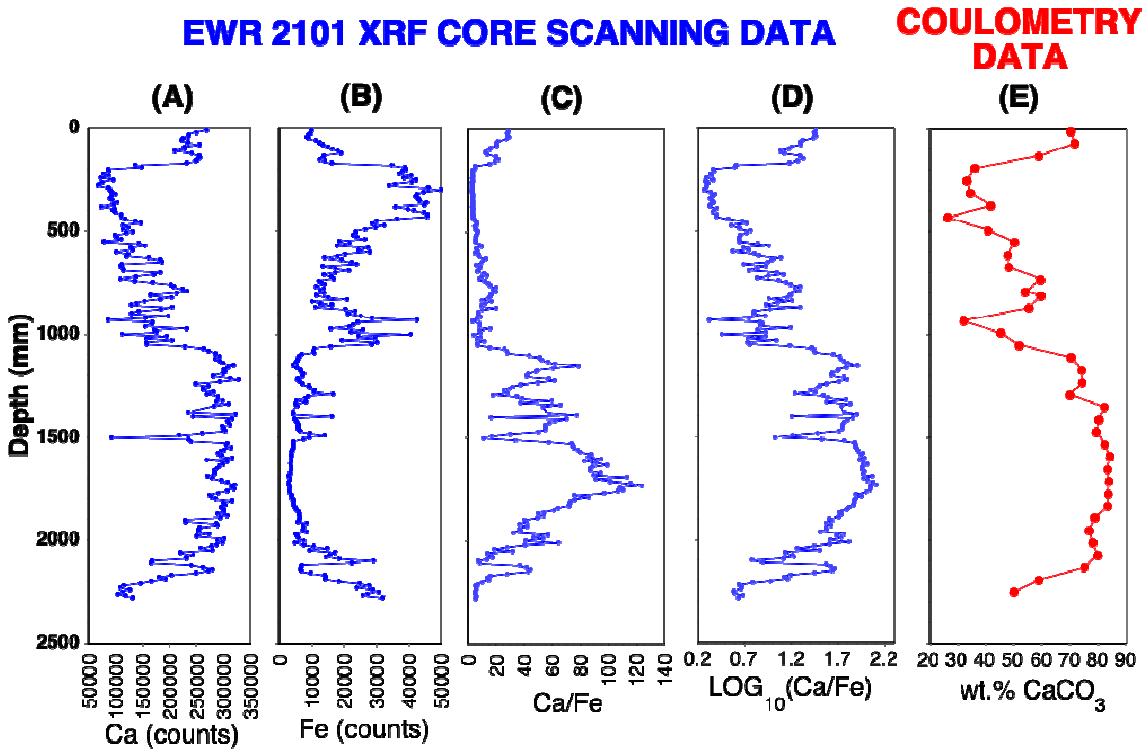

FIGURE 7. Reconstruction of changes in $CaCO_3$ contents for EWR 2101: Estimation of wt.% $CaCO_3$ for core EWR 2101. A.) Raw XRF Calcium Counts B.) Raw XRF Iron counts C.) XRF Ca/Fe ratio D.) Log_{10} of XRF Ca/Fe ratio E.) Percent calcium cabonate measured via CO_2 Coulometry

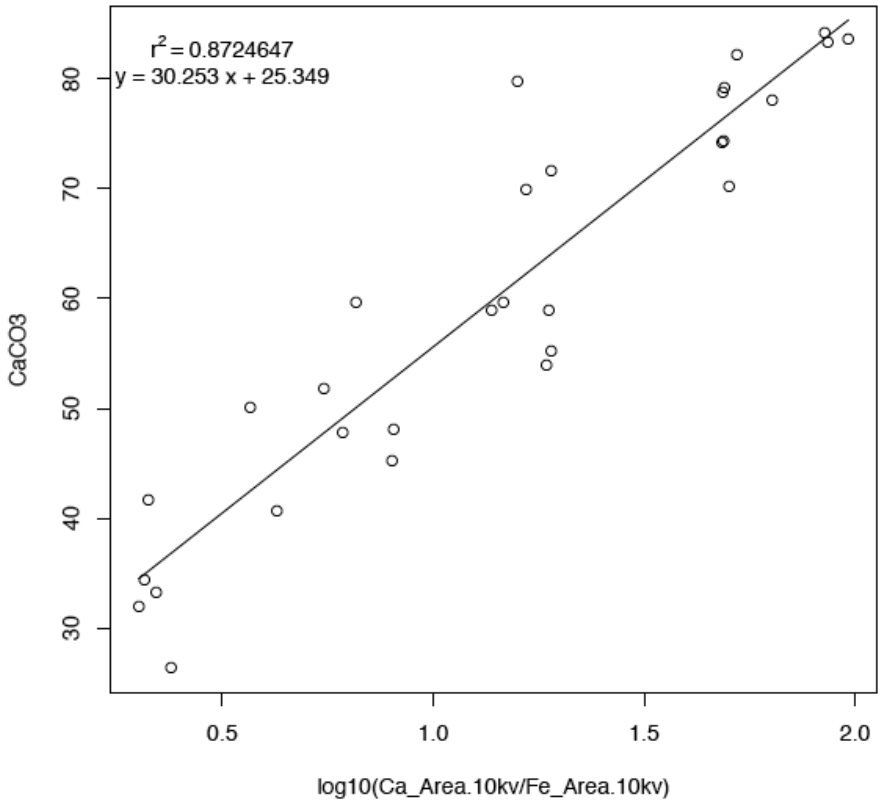

FIGURE 8. XRF Calibration of $CaCO_3$ contents for EWR 2101: Calibration of the XRF-derived Ca/Fe versus coulometrically-determined wt.% $CaCO_3$ data for core EWR 2101.

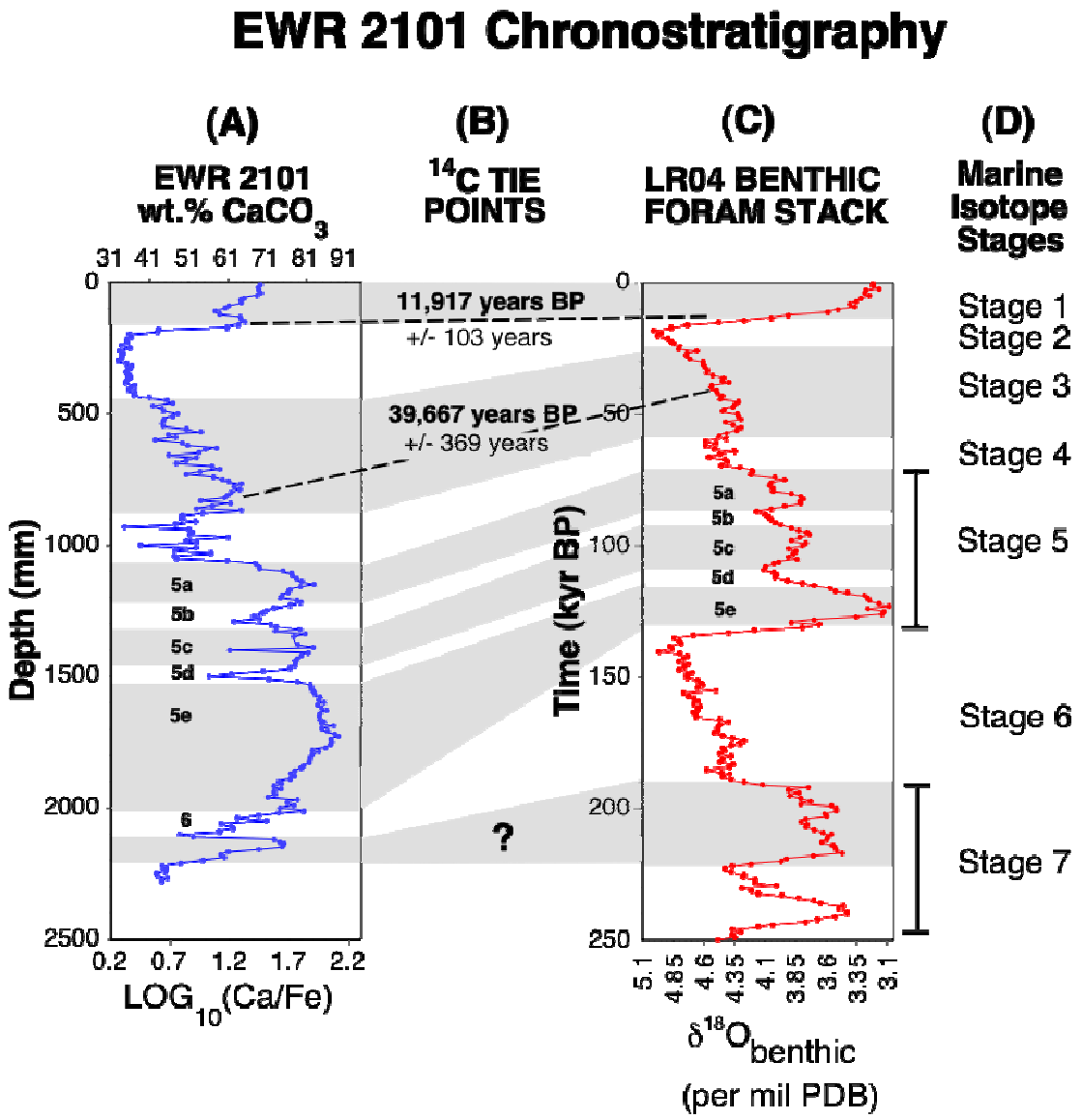

FIGURE 9. EWR 2101 Chronostratigraphy: Calibrated XRF %$CaCO_3$ results correlated to the LR04 benthic foraminifera stack (Lisiecki and Raymo, 2004). Wiggle-matching was performed on Analyseries (Paillard et al., 1996). Marine Isotope Stages after Imbrie et al. (1984). Details for the AMS radiocarbon dates are in Table 2.

Comparison of the high-resolution EWR 2101 wt.% $CaCO_{3\text{-}XRF}$ record to the LR04 stack is illustrated in Figure 9. In developing the chronostratigraphy for this site, I incorporate the temporal constraints provided by two intervals that have been dated via radiocarbon (Figure 9B; see Table 2). These radiocarbon dates anchor the EWR 2101 core at 150 mm depth to 11,917 calendar years, and at 810 mm depth to 39,667 calendar years. The identification of chronostratigraphic intervals equivalent to Marine Isotope Stages 1-5 are relatively unambiguous, however, the correlation of the lowermost interval of EWR 2101 (>200 cm depth) is uncertain, and thus the interpretation shown in Figure 9 is speculative. The chronostratigraphic interpretation proposed in Figure 9 indicates sedimentation rates (compacted) that range from ~3 mm/ka to ~60 mm/ka across stages 1-5, with no obvious propensity for higher sedimentation rates during the warm or cold intervals.

TABLE 2. Accelerator Mass Spectrometer radiocarbon results for planktonic foraminifera from core EWR 2101.

Depth	Radiocarbon Age	Standard Deviation (radiocarbon)	Calendar Age	Standard Deviation (calendar)
150mm	10200	50	11917	103
810mm	34300	330	39667	369

Samples were measured at the National Ocean Sciences Accelerator Mass Spectrometry Facility. A reservoir correction of 400 years was applied prior to conversion to calendar age following the method outlined in Fairbanks et al. (2005) (see http://radiocarbon.ldeo.columbia.edu/research/radcarbcal.htm)

4.2 RESULTS: Multi-proxy XRF-scanning analysis of EWR 2101

XRF core scanning of EWR 2101 is utilized to develop continuous 1-cm resolution records of seventeen distinct elements, including aluminum, silicon, sulfur, potassium, calcium, titanium, vanadium, chromium, manganese, iron, zinc, bromine, rubidium, strontium, zirconium, lead and barium. These elements were selected based on their utility for evaluating lithogenous, biogenic, and authigenic processes (see *Section 2.2*), and the ability to robustly detect them via XRF core scanning in EWR 2101 sediments.

Factor analysis has been utilized to summarize the overall geochemical variability documented in the XRF core scanning data, and to assist in the attribution of these elements to lithogenic, biogenic and authigenic sources. Table 3 summarizes the results, utilizing three factors with a Varimax rotation (all statistical analyses were performed in R; R Development Core Team, 2010). Three factors were retained based on evaluation of the factor analysis "scree plot" (Figure 10), which illustrates the relative amount of variance that is attributable to each of the 17 possible factors. In total, the 17 elements investigated contribute a total of 17 units of variance, 9.83 of which are accounted for by the first factor, 1.97 of which are accounted for by the second factor, and 1.21 units of which are accounted for by the third factor. In total, these three leading factors recover 77% of the variance in the data set, and they also rise above the "background scree" of factors 4-17, which can be approximated (to a first-order) by a line. The resultant factor scores for these three components (their variability with depth) are illustrated in Figure 11.

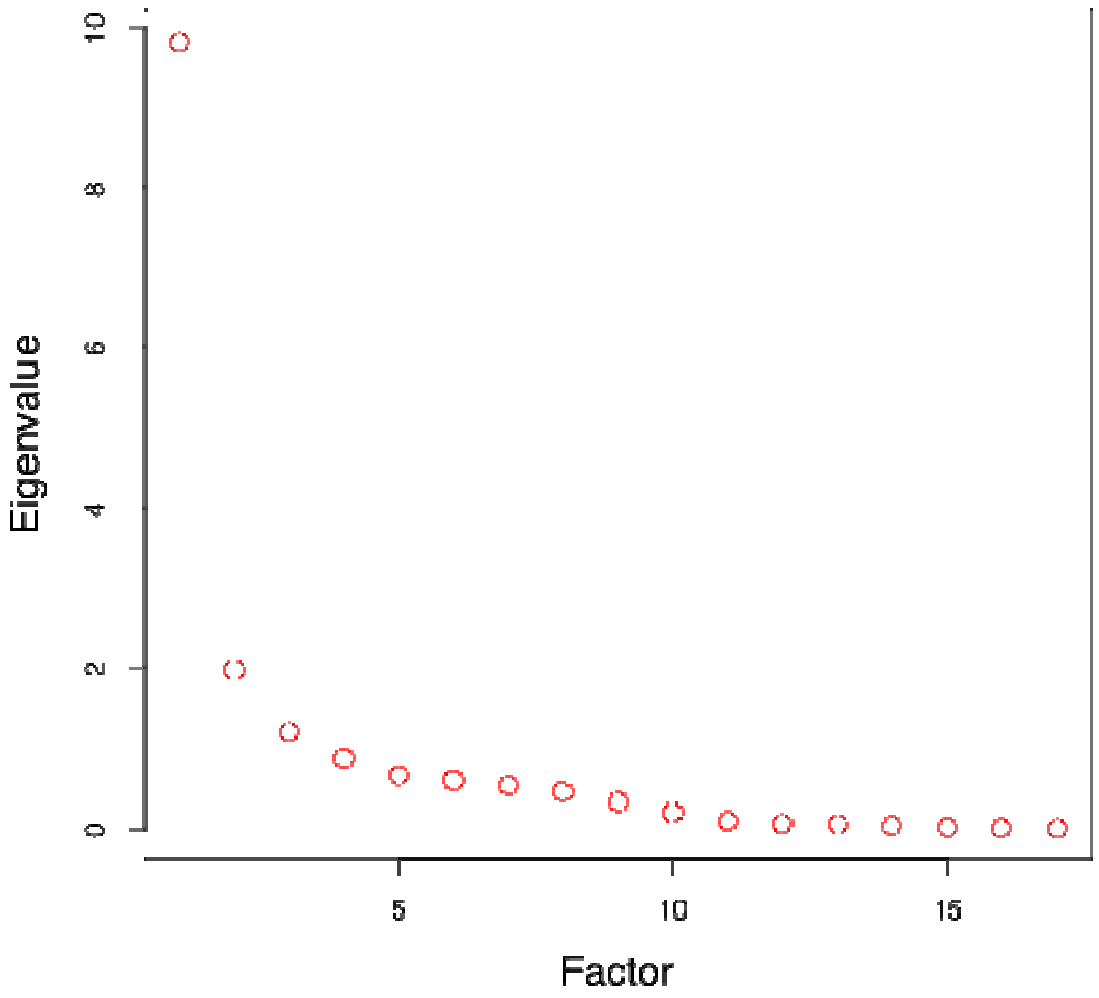

Figure 10. Scree Plot for factor analysis results: Scree plot (sorted factor analysis eigenvalues) for core EWR 2101 XRF scanning data. Factor 1 – Lithogenic vs. carbonate; Factor 2 - Marine organic matter bioproductivity and delivery; Factor 3 – Oxygen availability near the sediment-water interface.

Table 3. Factor Analysis Results for the EWR 2101 XRF-core scanning data.
Factor Analysis, 3 factors retained, Varimax rotation

R Call: principal(r = data, nfactors = 3, rotate = varimax, scores = T)

ELEMENT	FACTOR 1 LOADING	FACTOR 2 LOADING	FACTOR 3 LOADING	COMMUNALITY (EXPAINED VARIANCE)
Al	**0.96**	-0.13	-0.08	0.94
Si	**0.96**	-0.15	-0.08	0.95
S	-0.33	**0.69**	0.02	0.59
K	**0.96**	-0.11	-0.05	0.94
Ca	**-0.81**	**0.51**	0.05	0.92
Ti	**0.92**	-0.21	0.20	0.93
V	-0.19	0.31	**0.72**	0.64
Cr	-0.37	0.44	0.03	0.33
Mn	0.06	-0.03	**0.88**	0.78
Fe	**0.96**	-0.17	-0.02	0.96
Zn	**0.95**	-0.05	0.00	0.90
Br	0.21	**0.70**	0.17	0.56
Rb	**0.94**	-0.12	-0.03	0.90
Sr	**-0.76**	**0.52**	0.05	0.85
Zr	**0.86**	0.17	-0.10	0.77
Pb	**0.67**	-0.17	-0.10	0.49
Ba	**0.61**	**0.43**	0.05	0.56
Proportion of Variance	**55%**	**13%**	**8%**	

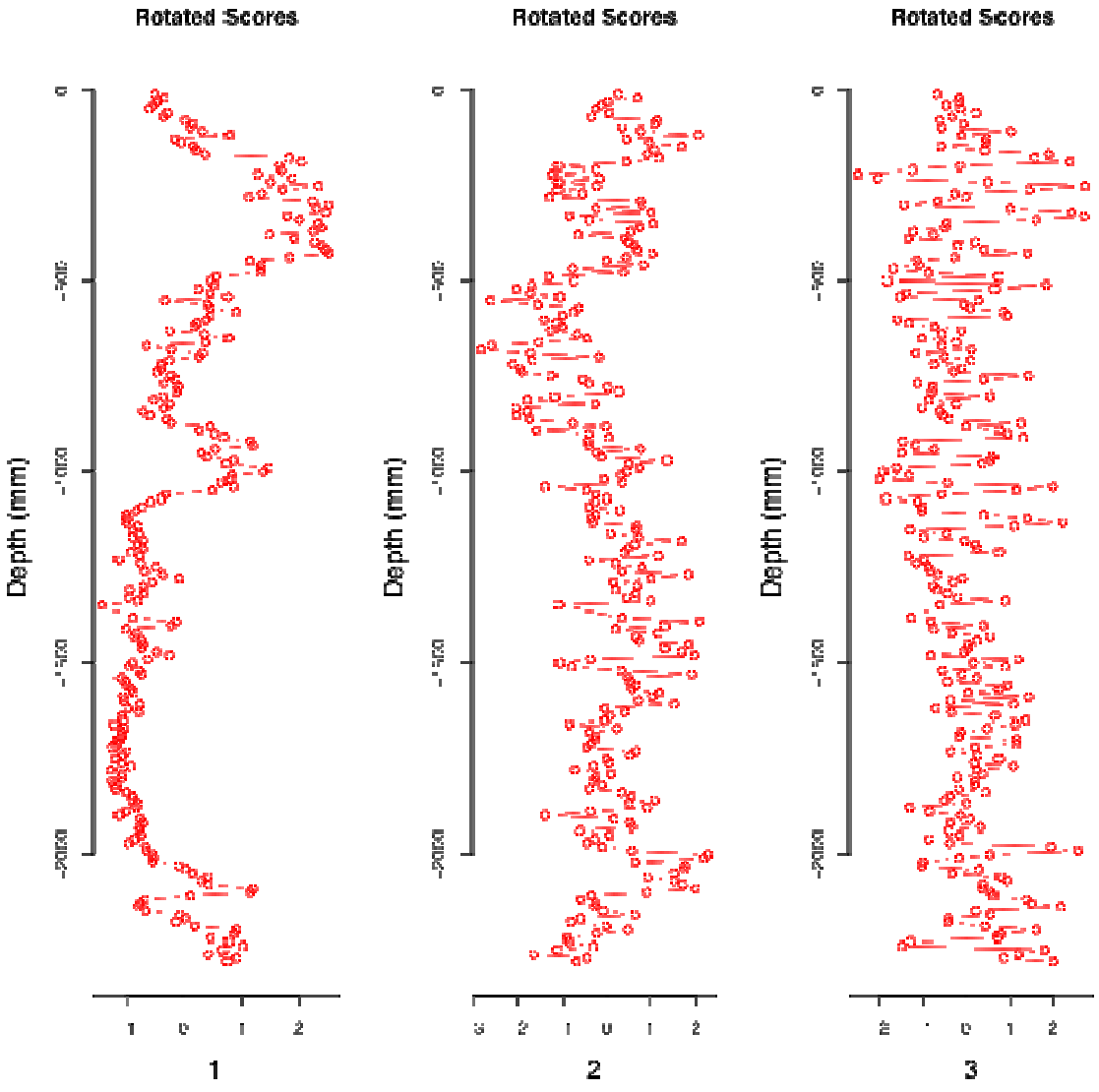

FIGURE 11. Factor analysis scores for the EWR 2101 XRF-core scanning data: Factor 1 is interpreted as reflecting lithogenic vs. carbonate contributions, factor 2 is interpreted as a organic matter bioproductivity and delivery factor, and factor 3 is interpeted to reflect oxygen content near the sediment water interface. See text for further discussion.

The first factor is characterized by large positive loadings (correlations) with lithogenous elements (Al, Si, K, Ti, Fe, Zn, Rb, Zr), and strong negative loadings with calcium and strontinum (Table 3, Figure 11, Figure 12). We thus interpret this factor as a lithogenous vs. carbonate factor, which tracks the overall pattern of climate evolution associated with marine isotope stages 1-5 (see Figure 1 and Figure 9). Factor 2 demonstrates highest loadings with bromine and sulfur. We interpret this factor to indicate changes in marine organic matter bioproductivity and delivery to the sediments (previous studies have demonstrated a strong covariation between bromine concentration and marine organic matter content; Mayer et al., 1981; Ziegler et al., 2008), and the production of sulfide by anoxic sulfate reduction within sediments (Jorgensen, 1977). The coupling of these two processes makes sense, as the availability of labile organic matter is a prerequisite for sulfate reduction (Berner, 1980). The third factor is characterized by highest loadings associated with manganese and vanadium, which can accumulate under oxic and suboxic conditions respectively (e.g. Froelich et al., 1978, Baes and Mesmer, 1976, Wehrli and Stumm, 1988). In fact, these two elements can accumulate simultaneously at any given time, although they are separated spatially in terms of their depth below the sediment water interface. Thus, we interpret factor three to represent changes in oxygen availability at or near the sediment water interface.

Past studies have utilized barium as measure of paleoproductivity (e.g. Schmitz, 1987, Shimmield et al., 1988, Paytan and Kastner, 1996; *Section 2.2*). At EWR 2101, this element shows substantial loadings on the first and second factor. The correlation of Ba content with the first factor could indicate a lithogenic source for some of the barium,

or alternatively, higher productivity during cold climate intervals. However, the loading of Ba content on factor 2 suggests a more complex relationship, perhaps reflecting changes in primary production of marine organic matter that are decoupled from the overall climate history. The substantial correlation of Ba, Br and S with factor two leads us to a tentative interpretation that the barium loading on factor two reflects changes in primary production, while the loading on factor one represents lithogenous barium. A summary of our interpretation of select XRF scanning data, based on the factor analysis results, is illustrated in Figure 12.

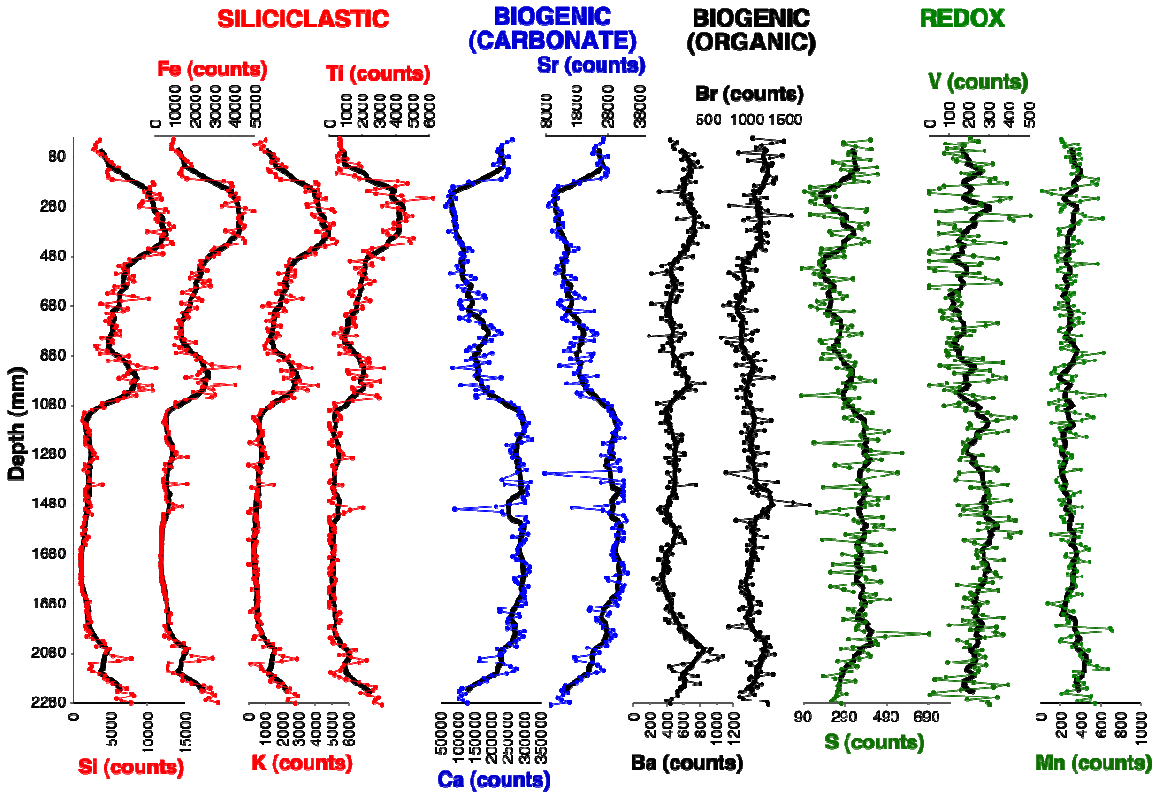

FIGURE 12. Interpretation of XRF elemental proxies from core EWR 210: Interpretations are based on factor analysis results. Bold black lines are 10 point moving averages.

4.3 RESULTS: Phosphorous speciation in EWR 2101

The SEDEX results for EWR 2101 are illustrated in Figure 13, and are briefly summarized here (note that organic phosphorous was not detected in the sediments, and thus is not included in the present discussion). The detrital phosphorous signal, which is largely comprised of igneous and metamorphic apatite, displays the expected covariation with lithogenic input (e.g., titanium content; Figure 13), resulting in generally higher concentrations during cold glacial intervals (marine isotope stages 2, 4, 5b, 5d). This fraction of phosphorous is not reactive and remains isolated from the dissolved pool. These results provide additional confirmation of the glacial/interglacial terriginous and carbonate regime shifts.

In contrast, Fe-bound phosphorous and authigenic phosphorous concentrations are less predictable. Iron-sorbed P is most abundant during stage 3, and stage 5B, with somewhat elevated values during stage 1 as well. Thus, somewhat surprisingly, Fe-bound phosphorous does not display a consistent relationship to bulk iron concentration (Figure 12) or climate state, although it is noteworthy that these three intervals of Fe bound phosphorous enrichment are characterized by relatively low bulk iron concentration. I will return to this issue in *Section 4.4*, however it is worth noting that this would suggest that a significantly larger portion of phosphorous is trapped in the sediments during warm stages 1 and 3 and cooler stage 5B, and thus, less P is released to the water column to sustain primary production.

The results of the phosphorous extraction associated with authigenic minerals are less definitive, largely due to difficulty associated with colorimetric measurement and potential batch effects (see the point-to-point oscillations between 1000 and 2000 mm depth, which are associated with two different batches). However, we can conclude that most of the phosphorous present in EWR2101 sediments is in the form of authigenic CFA. Furthermore, there is no obvious relationship to climate state.

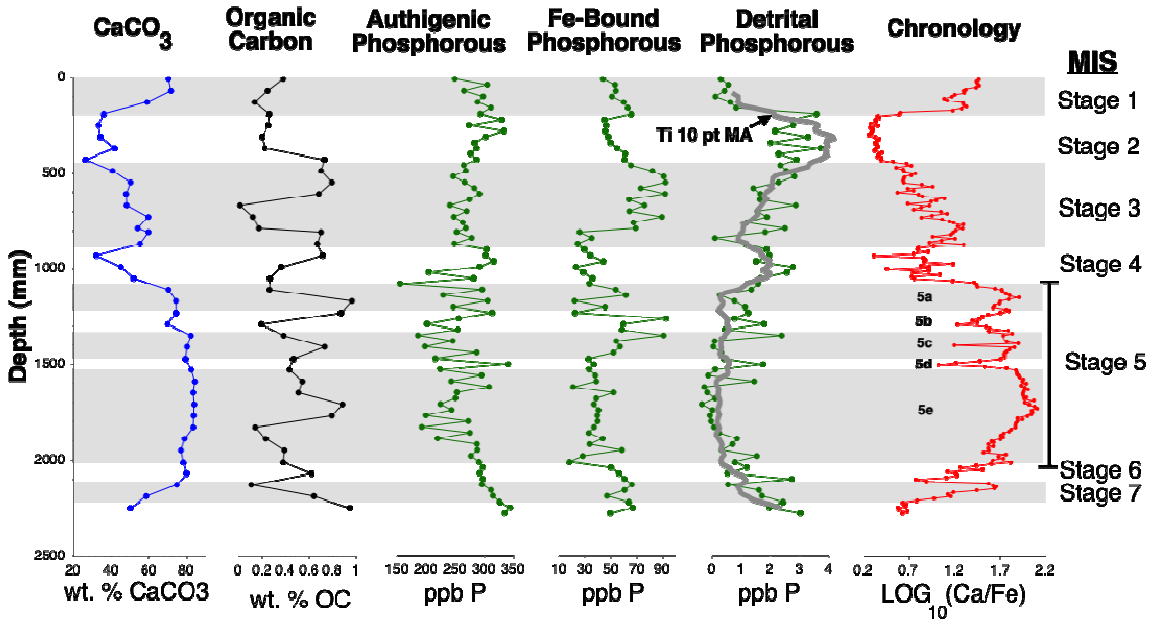

FIGURE 13. Coulometer and P extraction data for core EWR 2101: %$CaCO_3$ and %OC measured via CO_2 coulometry; SEDEX-derived P_{auth}, P_{Fe}(sorbed) and $P_{detrital}$; Chronology based on calibrated Ca_{XRF} results (see Figure 9).

4.4 RESULTS: Interpretation of the depositional history at EWR 2101

In this section, I provide a synthesis of select XRF core scanning proxy data and phosphorous speciation data, with the goal of interpreting the paleoenvironmental history of EWR 2101. To facilitate this discussion, I highlight my primary interpretations with respect to the Marine Isotope Stages (Figure 14I):

(1) Stage 5e: This interval is characterized by high wt.% $CaCO_3$ and low lithogenic contents (Figure 14 A and B). Inferred primary productivity (Figure 14C and D) generally declines from the base of this interval towards the middle, then recovers slightly towards the top. This interval has the highest sulfide contents of the record (Figure 14E), and the lowest Fe-bound phosphorous contents (Figure 14F), consistent with more reducing pore waters. This observation is broadly consistent with manganese abundance (Figure 14G), which displays the lowest values of the record (although variable).

(2) Stages 5a-d: This interval includes two oscillations of increasing/decreasing wt.% $CaCO_3$ (Figure 14A). Sulfide concentrations remain high and relatively steady from Stage 5e (Figure 14D), and inferred primary productivity displays only minor variability (Figure 14C and D). However, the center of this interval is characterized by an increase in iron-bound phosphorous (Figure 14F), which may be attributable to a slight increase in primary productivity (Figure 14C).

(3) Stage 4: This interval is characterized by low wt.% $CaCO_3$ and high lithogenic contents (Figure 14A and B). The proxy data also suggest an increase in primary productivity (Figure 14C and D), coupled to an increase in sulfide production via sulfate reduction (Figure 14E). This interpretation is consistent with low iron-

bound phosphorous contents (Figure 14F) and low manganese concentrations (Figure 14G).

(4) Stage 3: This interval is characterized by intermediate and declining wt.% $CaCO_3$ (Figure 14A). Proxy evidence suggests a substantial decline in productivity from those values in stage 4 (Figure 14C and D), which is consistent with low sulfide contents (Figure 14E) and sustained high-levels of iron-bound phosphorous (Figure 14F). The sediment-water interface oxygen content appears to have been somewhat intermediate to those levels seen in earlier and later times (Figure 14G and H).

(5) Stage 2: This interval contains the lowest wt.% $CaCO_3$ of the record, and the highest amounts of lithogenic components (Figure 14A and B). Proxy data suggests a pulse of primary productivity in the middle of Stage 2 (Figure 14C and D), synchronous with increased sulfide production via sulfate reduction (Figure 14E). This interpretation is consistent with declining iron-sorbed phosphorous concentrations (Figure 14F). SWI oxygen content appears to increase in this interval, following the inferred productivity pulse (Figure 14H).

(6) Stage 1: This interval is characterized by high wt.% $CaCO_3$ and low lithogenic contents (Figure 14A and B). Although these sediments are quite different than those deposited during stage 2, the elemental proxies yield some similar interpretations for the paleoenvironment, with an inferred pulse of primary productivity (Figure 14 C and D) and sulfide accumulation (Figure 14E) in the middle of the interval. Relatively oxic conditions at the sediment-water interface (Figure 14G and H) occur at the base of this interval, but then decline. Finally,

there is evidence for intermediate levels of iron-bound phosphorous (Figure 14 F).

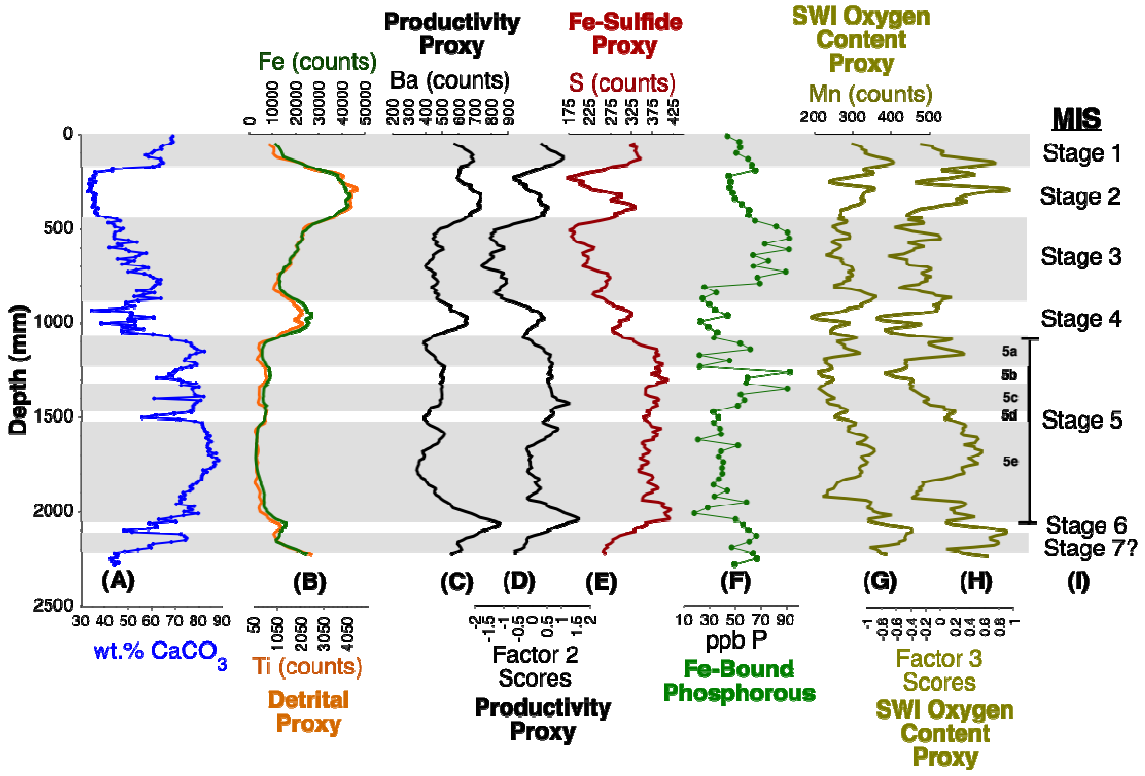

FIGURE 14. Summary figure for core EWR 2101: All plots are 10 point moving averages, with the exception of wt.% $CaCO_3$ and Fe-bound phosphorous data. A.) Calibrated wt% $CaCO_3$; B.) Detrital Proxy – XRF-derived Ti and Fe; C,D.) Productivity Proxy - XRF-derived Ba and Factor 2 scores; E.) Fe-Sulfide Proxy – XRF-derived S; F.) Phosphorous-sorbtion Proxy – SEDEX-derived P_{Fe}; G,H.) SWI Oxygen Content Proxy – XRF-derived Mn and Factor 3 scores

5. DISCUSSION AND CONCLUSIONS

The fundamental objectives of this study were (1) to document the glacial/interglacial response of marine sedimentation in the North Atlantic, with respect to select major, minor and trace elements that can be used to reconstruct changes in lithogenous, biogenic and authigenic processes, (2)
to test the hypothesis that the dominant glacial/interglacial sedimentologic shifts (clay versus calcium carbonate content) are also paralleled by changes in redox state and biogeochemical remineralization processes within the sediments, and (3) to test the hypothesis that enhanced iron delivery during glacial times diminished the regeneration of phosphorous to the water column by adsorption onto iron oxyhydroxides near the sediment-water interface, potentially impacting nutrient availability for primary productivity..

Regarding the first and second objectives, this study documents a number of key relationships between glacial/interglacial climate change and major, minor and trace element geochemistry. Of primary importance is the relationship established between climatic shifts and the inverse variation of detrital and carbonate depositional signals in the sediments of core EWR 2101. Comparison of the LR04 benthic stack with the calibrated XRF-derived Ca normalized to Fe on a $\log_{10}$ scale also shows the utility of XRF scanning as a means for rapid development of core chronology.

Factor analysis of the 17 elements measured via XRF scanning provides an estimate of the relative importance of lithogenous, biogenic, and authigenic controls on marine sedimentation at this site. The first factor reflects lithogenous vs. carbonate

sedimentation, which tracks the overall pattern of climate evolution associated with marine isotope stages 1-5. We interpret factor two as indicating changes in marine organic matter bioproductivity and delivery to the sediments. The dual nature of barium loading on both factors 1 and 2 may provide a robust method for discerning the fractions of detrital and biogenic Ba. At this site, factor 3 also shows promising results as an indicator of oxygenation state at or near the sediment-water interface.

When combined with the XRF scanning elemental data, the SEDEX results suggest a delicate (and variable) balance between primary productivity, redox state, and the ability of sediments to adsorb phosphorous. Much of the study interval shows strong, consistent trends closely coupled with regional/global climate. For example, the warmer periods, as illustrated by interstadial Stage 3, are typically carbonate-dominated, iron-poor and sulfur-poor, with relatively low productivity and high adsorbed phosphorous content. Stages 2 and 4, which are colder periods of the last glacial, display trends that are anti-phase to Stage 3 (siliciclastic dominated, high productivity, high sulfide and low sorbed phosphorous), suggesting a linkage between regional/global climate and the chemistry of ocean sediments. Stages 5b, 5c, and the transition between Stages 1 and 2, however, show a decoupling of P_{sorbed}, redox conditions and regional/global climate, indicating that a complex relationship can develop, possibly due to local climatic or oceanographic factors.

Regarding objective 3, our results do not suggest that enhanced iron delivery during glacial times (e.g., the peak iron concentrations of stages 2 and 4) diminished the regeneration of phosphorous to the water column by adsorption onto iron

oxyhydroxides. As discussed above, our results provide evidence that the phosphorous sorption capacity of North Atlantic sediments from the Rockall Plateau was primarily linked to redox conditions throughout the past ~125,000 years. This interpretation is supported by results from the North Sea (Slomp et. Al., 1996) and the North Atlantic Gateways (Tamburini, 2001), which show a strong correlation between pH, oxygen levels, alkalinity and the P-sorbtion capacity of sediments. Slomp et al. (1996) suggests that this linkage is likely established due to the influence of these factors on the distribution of amorphous iron-oxides in the sediments. They suggest that dysoxic to anoxic conditions, which cause dissolution of amorphous iron-oxides, strongly inhibit retention of P in sediments. Interestingly, our results do not indicate a positive correlation between bulk iron content and Fe-bound phosphorous, suggesting that the iron oxide content of sediments on the Rockall Plateau is not strongly coupled to the bulk iron flux.

APPENDIX A: Coulometry Results

Carbonate and Organic Carbon measured via CO_2 Coulometry.

Depth (mm)	%CaCO3	%Organic Carbon
10	70.31	0.37
70	71.67	0.24
130	59.02	0.13
190	36.055	0.26
250	33.31	0.25
310	34.51	0.20
370	41.77	0.23
430	26.41	0.73
490	40.75	0.70
550	50.23	0.80
610	47.87	0.68
670	48.16	0.01
730	59.66	0.12
790	54.00	0.17
810	59.72	0.70
870	55.26	0.67
930	32.07	0.72
990	45.25	0.36
1050	51.91	0.27
1110	70.35	0.26
1170	74.25	0.97
1230	74.40	0.87

1290	69.97	0.19
1350	82.27	0.38
1410	80.20	0.73
1470	79.33	0.47
1530	82.43	0.43
1590	84.30	0.54
1650	83.47	0.51
1710	83.98	0.88
1770	83.69	0.80
1830	83.51	0.14
1890	78.84	0.23
1950	76.93	0.39
2010	78.20	0.38
2070	79.81	0.62
2130	75.14	0.11
2190	59.01	0.65
2250	50.13	0.95

APPENDIX B: SEDEX Results

Phase-specific Phosphorous data measured by a modified version of the SEDEX Method (Ruttenberg, 1992)

Depth (mm)	Fe-bound P (ppb)	Authigenic P (ppb)	Clay-bound P (mMol/L)
10	43.61	248.50	0.29
40	52.80	303.93	0.54
70	53.44	264.02	0.41
100	50.42	296.95	0.10
130	59.50	287.43	0.61
160	62.60	310.28	0.81
190	65.45	292.25	3.57
220	45.04	329.03	2.76
250	46.34	273.01	2.78
280	45.61	332.55	2.17
310	47.86	301.85	3.28
340	49.70	282.43	1.99
370	54.52	285.60	3.73
400	60.91	275.67	2.28
430	60.36	285.46	2.90
460	65.04	263.81	2.33
490	81.50	267.27	2.53
520	90.38	245.69	2.80
550	91.71	265.18	2.26

580	72.68	281.84	1.40
610	91.45	290.82	1.64
640	63.44	273.56	1.62
670	75.53	240.12	2.85
700	63.77	268.56	1.54
730	88.95	246.89	1.86
760	66.96	261.93	1.17
790	68.72	267.30	2.49
810	25.43	251.69	1.81
840	34.76	277.39	0.09
870	24.03	247.755	1.12
900	29.37	303.31	1.87
930	33.82	301.40	1.96
960	44.05	315.14	1.51
990	22.83	290.94	2.77
1020	28.68	203.99	2.56
1050	35.46	280.63	1.65
1080	33.16	154.70	1.56
1110	53.40	295.39	1.33
1140	61.26	228.56	0.26
1170	21.70	304.59	0.75
1200	45.07	246.13	1.12
1230	22.05	312.61	1.24
1260	92.31	255.47	0.76
1290	59.39	200.73	1.78
1320	58.16	253.67	0.44

1350	90.33	185.39	2.38
1380	53.80	245.30	0.08
1410	56.75	197.34	0.03
1440	51.65	286.14	0.31
1470	32.57	215.06	0.43
1500	36.63	340.04	1.74
1530	32.85	223.76	0.10
1560	37.66	294.37	-0.15
1590	38.46	242.46	1.44
1620	20.54	307.10	-0.28
1650	51.65	252.11	-0.18
1680	38.44	249.73	0.09
1710	36.58	223.75	-0.36
1740	40.17	243.06	0.00
1770	39.25	198.73	-0.08
1800	39.51	271.68	-0.05
1830	36.69	192.02	0.06
1860	32.58	274.28	0.23
1890	43.29	218.86	0.85
1920	33.25	286.58	0.69
1950	58.27	287.26	0.32
1980	27.91	276.12	1.52
2010	17.66	290.12	0.77
2040	49.91	296.63	1.19
2070	55.96	291.08	0.54
2100	60.44	296.49	2.7

2130	66.03	295.75	0.54
2160	60.47	311.17	1.60
2190	46.83	314.58	1.71
2220	63.66	325.78	2.4
2250	66.76	343.71	1.96
2280	49.32	334.20	3.03

APPENDIX C: XRF Qualitative Bulk Geochemistry Data

XRF data collected by an Avaatech XRF Core Scanner. Cores were scanned sequentially across the spectrum of voltage levels to ensure consistent sampling locations on the sample. Data is given in photon counts.

5kV Data

Depth (mm)	Al	Si	S	Cl	K	Ca
10	264	3603	415	6785	1026	50642
20	201	3125	283	6028	673	45409
30	160	2951	283	5522	374	43060
40	111	2992	338	5392	892	43720
50	172	2725	417	5432	699	42961
60	222	3223	311	5188	946	41177
70	230	3792	308	6480	1509	43890
80	217	4373	337	7730	1559	47980
90	407	4578	412	6871	1735	42481
100	447	5035	229	6787	1379	40512
110	344	5376	281	6024	1975	39399
120	417	5985	443	7110	2202	44770
130	339	4747	271	7635	1167	46279
140	288	4508	317	7403	1298	47382
150	337	4640	448	6526	1605	47297
160	246	4665	330	7210	1637	46181
170	365	5167	333	6659	1888	43336
180	924	10741	405	5622	4040	24753
190	951	10875	248	5541	4209	25757
200	865	10333	121	4174	3401	14163
210	930	10265	235	3839	4173	16175
220	990	9454	94	3745	3401	13512
230	1086	11596	133	4933	4274	15280
240	1023	9944	242	4292	4132	13200
250	1142	11885	149	4594	4638	16793
260	837	9276	124	4108	4052	13976
270	713	9025	143	3201	3489	12971
280	771	8784	215	3390	3527	12675
290	1040	12343	397	5008	4987	15707
300	1111	12787	389	5142	5147	16241
310	1044	11373	120	5699	3796	14769
320	894	11481	190	4766	3963	16955
330	928	11154	275	4174	4272	16417
340	933	11357	282	4242	4431	16317
350	1158	12890	401	4599	5059	18129

360	1190	13624	357	5420	4856	18563
370	1112	13042	368	5384	4832	17549
380	853	9991	215	4220	4096	14322
390	1057	12133	225	4363	4583	18369
400	1072	11884	316	4547	4492	17656
410	1204	12574	383	4841	5029	17443
420	1111	13194	407	5356	5312	20255
430	1148	13423	365	5354	5211	20500
440	966	11933	290	4477	4573	21972
450	696	10145	176	5177	3716	25768
460	810	10504	282	4579	3617	27579
470	945	12036	174	4108	4015	21331
480	700	9537	286	3820	3374	22690
490	639	7538	181	3501	2463	19732
500	585	7715	169	3598	2412	24015
510	504	7001	167	3242	2418	21809
520	467	6059	176	3227	2237	17962
530	510	6841	81	2715	2545	19263
540	575	7370	207	3785	2795	20600
550	431	5695	138	2139	1776	12698
560	572	8054	171	3596	2740	26441
570	470	7541	327	3982	2212	28088
580	567	8115	234	3759	2562	23432
590	492	7256	143	3324	1870	22816
600	463	5506	217	3552	2089	18369
610	498	6502	183	3227	2195	22657
620	372	5308	235	3290	1835	22497
630	320	4548	262	4085	1684	30421
640	618	8036	298	4877	2532	34228
650	897	10173	279	4728	3192	33967
660	407	6427	153	3502	2248	19916
670	244	3758	190	2750	1239	19442
680	290	4573	124	2427	819	19336
690	569	7260	156	3920	2084	20738
700	436	6755	331	4557	2170	32719
710	330	4471	192	4170	1314	31267
720	344	5253	207	3270	1728	25071
730	386	4918	256	2647	1510	19630
740	332	4312	232	2822	1035	24750
750	308	4849	225	3585	1516	31848
760	403	5738	321	4892	1898	36867
770	398	5501	303	4704	1134	36525
780	401	6294	256	5099	1216	39705
790	406	5586	367	5638	1712	42431
800	480	6354	311	4259	1820	38349
810	298	3890	265	4857	1596	31535
820	360	5167	171	5628	1206	35443
830	428	5147	180	6222	1052	31809
840	180	2909	261	3975	944	27553

850	170	3131	212	4144	952	24854
860	360	4594	285	3525	1575	24117
870	209	3616	186	6195	1150	38029
880	624	7453	310	6638	2450	34170
890	553	6109	177	4407	2306	26748
900	326	4684	283	6032	1804	22807
910	628	7589	338	6733	2645	36903
920	761	8597	334	5849	3050	28815
930	898	11104	248	4907	3797	14940
940	696	7681	317	6486	1936	29253
950	564	7312	318	5670	2676	30832
960	531	6955	310	5461	2581	28477
970	492	6077	361	6718	2091	40259
980	724	8157	436	6790	3053	31481
990	717	7777	279	5912	2856	31998
1000	1014	10603	313	5656	4192	20793
1010	797	8819	335	5140	2906	35816
1020	880	10720	254	5766	3527	28422
1030	478	6937	259	5724	1489	35191
1040	747	8458	78	5762	2551	27324
1050	490	6786	354	6738	2720	28685
1060	432	5881	311	6485	2061	41695
1070	272	3957	290	7134	1425	47644
1080	213	3813	326	8031	1342	50059
1090	350	4093	280	7627	1259	52296
1100	120	2459	351	7497	781	53582
1110	78	1454	421	7080	685	53696
1120	85	1411	337	7309	604	52573
1130	69	1311	287	8565	280	52853
1140	60	1253	324	9069	418	54485
1150	137	1417	374	8916	545	57597
1160	108	1733	380	8945	645	57162
1170	113	1825	393	8485	651	55087
1180	162	2151	500	8511	822	56745
1190	74	1937	478	8287	792	54563
1200	81	2188	364	7620	795	51749
1210	49	1502	370	8079	600	57563
1220	126	1711	449	8848	531	60818
1230	110	1573	137	7779	68	51938
1240	97	1700	359	6958	593	44666
1250	207	2210	373	8593	897	49455
1260	105	2475	414	7773	806	46357
1270	80	2727	564	8236	1006	48357
1280	154	2695	388	8642	1023	51159
1290	205	3184	398	8665	1139	49458
1300	50	2517	464	8635	814	53003
1310	150	2278	388	8102	816	53757
1320	156	1512	240	8498	-1	53234
1330	107	1904	311	8697	432	51420

1340	53	1371	402	8763	527	56596
1350	83	1858	543	9040	669	50991
1360	79	4759	137	2351	93	10933
1370	56	1711	71	134	-211	2229
1380	87	2142	350	6423	571	42162
1390	175	2095	374	8779	587	59623
1400	301	3915	383	8492	1521	44697
1410	142	1889	185	9357	164	56089
1420	80	1649	408	8776	503	56040
1430	86	1642	381	9006	516	55901
1440	144	1663	341	9303	447	56978
1450	130	1880	496	9335	477	54598
1460	115	1565	450	9231	496	55319
1470	97	2018	386	9264	637	55015
1480	156	2288	447	8495	658	46286
1490	167	2293	386	8892	641	40110
1500	92	1536	261	4472	140	16278
1510	59	1969	151	7546	-30	40640
1520	138	2420	299	7990	393	42810
1530	88	1486	467	8894	434	56502
1540	131	1527	331	10311	424	54536
1550	71	1407	354	8900	513	57993
1560	73	1391	470	8372	553	56594
1570	112	1195	433	8184	562	54275
1580	95	1612	524	8268	313	52856
1590	77	1515	407	8315	471	54216
1600	72	1176	294	8945	371	58734
1610	94	1935	386	9193	289	47758
1620	70	1717	181	9627	-211	56195
1630	63	1437	351	8749	453	56313
1640	71	1585	461	8230	370	53629
1650	81	1133	347	7995	342	52398
1660	12	995	355	7985	304	51787
1670	66	1072	484	7433	299	52410
1680	125	977	276	6941	319	52536
1690	20	953	344	7567	435	50715
1700	41	981	374	7858	280	50895
1710	103	1132	375	8126	440	54920
1720	62	1015	229	9115	-122	56522
1730	72	1079	428	8549	394	59043
1740	122	1093	430	8636	566	58582
1750	51	1139	219	7786	340	58175
1760	81	1006	363	8548	507	57821
1770	124	1223	388	7876	464	54386
1780	53	1005	391	6930	319	50737
1790	80	1034	461	6766	431	51795
1800	80	963	328	7147	435	52395
1810	47	1204	219	7675	503	56457
1820	44	1169	285	8082	184	54072

1830	63	1169	330	7062	544	55836
1840	39	1296	439	7434	547	54464
1850	39	1593	383	8354	569	55195
1860	161	1733	504	9050	543	54792
1870	149	2204	414	8630	578	52990
1880	118	1832	366	8235	543	54747
1890	46	1808	387	7205	490	51692
1900	41	1848	307	4465	325	41758
1910	167	1754	330	5181	93	41495
1920	109	1995	387	9677	617	50708
1930	86	2045	375	8522	440	51904
1940	98	2041	282	6809	539	45735
1950	71	2349	389	6650	666	45600
1960	99	1968	356	8470	751	46789
1970	81	1583	350	8448	515	49594
1980	98	1771	341	7081	613	44129
1990	110	1999	382	8791	681	54334
2000	235	2253	694	9972	766	52991
2010	154	1827	482	9606	350	55199
2020	172	2573	308	8715	299	51704
2030	223	3971	438	8425	1162	52212
2040	251	4197	448	8555	1473	47618
2050	206	2996	327	8654	858	50126
2060	411	4844	270	7393	1846	40534
2070	321	4468	374	7376	1565	44687
2080	238	4285	404	8687	1548	43226
2090	431	5296	413	7879	2032	42573
2100	643	7830	355	7427	2901	31282
2110	503	5958	252	5525	1962	31077
2120	151	2239	319	5829	123	42026
2130	172	2418	347	6766	695	47815
2140	76	2156	273	6920	770	50973
2150	173	2499	317	7528	914	50727
2160	200	3450	267	6925	1214	46458
2170	353	4296	184	6364	1569	37690
2180	339	4174	241	5029	1449	33363
2190	224	4592	338	5315	1331	34577
2200	358	5282	259	5255	2033	30194
2210	646	6331	253	4879	1777	25392
2220	548	7170	264	4460	2509	21022
2230	498	5885	250	3826	2304	20619
2240	726	7846	298	5324	2786	23644
2250	596	8105	246	5202	2971	20487
2260	494	5791	237	4430	2377	18638
2270	534	6473	223	4461	2332	21694
2280	670	7781	272	6404	2813	23634
2290	438	5330	425	5621	2041	15212
2300	31	97	55	979	-156	42

10 kV Data

Depth (mm)	Al	Si	Cl	K	Ca
10	421	5855	11930	3169	265848
20	415	5373	10482	2801	248039
30	363	5121	9847	2633	233128
40	310	4741	10395	2574	231478
50	317	4437	9562	2311	223219
60	298	5362	10435	2871	219979
70	354	6184	11746	3179	231077
80	210	7210	13004	3490	253674
90	473	7788	12778	5662	224960
100	427	8884	12157	3961	224743
110	732	9106	11994	6468	207741
120	888	10337	12997	7286	238591
130	495	8267	13296	4076	252779
140	748	7906	13085	4111	253998
150	490	7959	11760	3316	250118
160	726	8157	12568	5757	246507
170	769	9250	12075	6494	229192
180	1925	18358	10683	12269	133970
190	1890	19527	10763	13387	144996
200	2021	19035	7927	11933	85141
210	1684	18220	8962	9965	85271
220	1300	18267	8590	9373	76763
230	1904	20864	10263	11302	85169
240	1836	17931	8241	11847	71526
250	2076	20557	9112	13519	92603
260	1700	17070	8220	12266	74535
270	1676	15474	7420	10009	68994
280	1500	15357	8227	9475	64117
290	2040	21927	9947	13301	85181
300	2372	23030	11118	14160	87892
310	2050	20851	9810	13438	91170
320	2022	20996	9205	13746	96564
330	1824	20014	8761	13264	90365
340	2079	20711	9131	13700	87274
350	2406	22577	9456	13318	92527
360	2412	23651	10732	13609	100022
370	2274	22780	11256	13011	93746
380	1743	17488	9022	10718	72316
390	2230	21593	9199	12250	95764
400	2166	21278	9768	12202	93124
410	2475	23147	10025	15884	97009
420	2199	23369	10582	15303	108649
430	2455	23685	10379	15557	108245

440	1990	20571	10103	12664	115977
450	1447	16971	9972	9408	134469
460	1203	17352	9670	8316	143776
470	1645	19696	8868	10233	111327
480	1548	16061	8511	9330	121125
490	1238	13833	7287	8880	111824
500	971	13331	7092	5497	129491
510	976	11827	6343	7480	118553
520	884	10036	6287	6972	96112
530	858	11622	6880	5638	99268
540	1137	12612	7859	6842	108985
550	947	10724	5478	5364	77155
560	1120	13624	7194	7449	140755
570	1019	12900	7720	6885	152609
580	1206	14642	7843	9175	126162
590	1125	12864	7349	8148	129129
600	745	8947	7825	5082	98981
610	846	11579	7869	5286	121698
620	644	9383	6786	4313	118803
630	604	7993	8715	3893	159888
640	1099	13654	8175	6672	180568
650	1390	17295	8788	9755	183580
660	1054	11098	7401	7443	109652
670	588	7244	7037	4252	106050
680	697	8386	5574	5586	111438
690	1297	13063	7459	6787	113766
700	1098	11957	9035	6064	180740
710	405	7939	8247	3400	169328
720	857	9751	8178	4416	135022
730	847	8393	6103	5310	107118
740	630	7451	5728	4221	133624
750	522	8201	7325	4896	167254
760	754	10032	9392	6032	200341
770	724	9692	8809	4506	206434
780	737	11043	9038	4199	221398
790	567	8974	9744	2667	228983
800	936	11311	8598	6153	210671
810	561	6647	9423	3765	163383
820	701	8924	12160	5142	202053
830	589	9046	11493	3628	180437
840	243	4764	7670	2342	151850
850	374	5578	8560	2217	136476
860	713	8223	7961	4291	127190
870	457	6339	12051	2942	203507
880	1304	12576	11965	6920	181626
890	1061	10777	9574	7204	140763
900	827	8612	12956	6061	127178
910	1219	13122	12282	8747	195185
920	1498	14737	11984	8166	153300

930	2187	20367	11875	11608	84461
940	998	14117	12826	5948	166593
950	977	12738	12466	5966	165146
960	1207	12499	10607	8241	152432
970	936	10589	13507	6869	229176
980	1353	14175	12681	9715	169874
990	1379	13068	11914	8117	173931
1000	1662	19457	13368	10057	109856
1010	1371	15356	10840	7651	191644
1020	1455	18748	10967	8232	154361
1030	1003	12270	11712	7727	203234
1040	1451	15589	10884	10528	154734
1050	1140	11905	13030	8332	155238
1060	881	9975	11280	6632	225349
1070	519	6600	12860	2342	260452
1080	284	6369	14437	3121	269542
1090	414	6934	13886	3990	282588
1100	120	4332	14232	2915	282758
1110	104	2477	13701	2226	289975
1120	55	2186	13050	2484	282137
1130	9	2362	14106	2287	290634
1140	113	1972	15911	2143	296302
1150	31	2379	17314	-2404	315439
1160	-13	2708	15236	151	305642
1170	69	2735	13722	589	298769
1180	244	3329	15126	2498	301029
1190	93	3320	15149	3015	297301
1200	153	3624	13671	2794	277878
1210	116	2720	15013	2414	310093
1220	20	2728	18397	1749	324698
1230	67	2720	12768	121	290952
1240	201	2835	12407	857	247105
1250	211	3682	15660	2329	268783
1260	224	4465	15127	3346	259233
1270	288	4325	14588	3547	260368
1280	268	4589	16236	3567	277669
1290	493	5412	16051	4037	266744
1300	180	4257	15442	2729	287005
1310	172	3808	14507	2402	286995
1320	26	2463	14999	1689	296011
1330	123	3281	14911	2010	283565
1340	135	2320	14617	2129	306606
1350	127	2955	16837	2118	279230
1360	143	9376	5424	413	61496
1370	84	3467	1100	-446	12166
1380	125	3830	12843	1025	231725
1390	152	3258	15605	1653	318817
1400	460	6910	16274	4896	240998
1410	221	3347	16173	2146	312284

1420	167	2781	16111	2521	304851
1430	103	2718	16610	2260	307083
1440	66	2587	16504	2447	309177
1450	96	2805	17375	1898	296192
1460	104	2524	17023	734	298406
1470	95	3422	16180	1562	301364
1480	90	3820	16096	1481	258054
1490	185	3706	16552	2206	215275
1500	39	2710	9072	900	90131
1510	111	3760	15663	2203	232490
1520	202	4230	15306	1822	236742
1530	-78	2519	16899	947	304685
1540	117	2699	17459	1263	302927
1550	42	2160	16072	1608	311317
1560	77	2171	15659	2108	299295
1570	15	2142	15327	1792	293438
1580	136	2833	15808	1739	286545
1590	95	2461	16045	2073	294218
1600	96	1731	16161	703	312817
1610	92	4033	16267	1183	266846
1620	21	2760	17354	2166	303972
1630	134	2554	17309	3159	297219
1640	233	2635	15225	1830	290058
1650	38	2102	13806	1614	284485
1660	87	1710	13481	1437	279546
1670	4	1572	13532	856	281313
1680	111	1761	13390	898	279858
1690	36	1396	14432	2478	267325
1700	162	1511	13393	1387	275911
1710	89	1703	14478	1679	293741
1720	58	1553	15598	1956	305276
1730	13	1763	17166	2315	317506
1740	21	1531	15385	1643	312611
1750	61	1944	15746	1104	316166
1760	25	1569	16827	1617	304674
1770	123	1933	12750	1683	287978
1780	78	1453	12016	1650	271118
1790	32	1628	11703	1517	275013
1800	26	1248	13367	1455	282310
1810	5	2199	14179	1049	313413
1820	32	1954	15039	-90	297273
1830	-18	1881	13261	1195	300537
1840	22	2131	13135	1921	293915
1850	134	2553	15670	2410	298491
1860	216	2867	16030	2742	298766
1870	106	3620	14988	663	285757
1880	179	3432	17272	-694	304524
1890	-2	2950	13313	1309	291980
1900	124	3260	9930	1414	226132

1910	135	2990	8567	2064	226609
1920	212	3597	15803	2971	283824
1930	296	3517	15700	2735	286765
1940	127	3572	11908	2231	254172
1950	199	3795	10920	1483	251526
1960	184	3102	16261	2297	252176
1970	63	2704	15143	-69	270067
1980	140	2826	13356	2356	249014
1990	185	3482	17365	2741	299223
2000	366	3944	18944	2954	285517
2010	303	2680	19552	2891	295867
2020	208	4454	17309	3343	284280
2030	415	6431	16005	4096	274415
2040	376	7031	16263	5537	255358
2050	351	4897	15416	3268	275908
2060	735	8637	13619	5838	217921
2070	499	7524	15358	5388	241255
2080	603	7437	16118	5529	229064
2090	657	9092	15473	6295	227986
2100	1218	13468	14435	8521	165902
2110	968	10201	11045	6984	164432
2120	273	3887	10526	2599	237826
2130	215	3865	11503	2503	259603
2140	238	3691	13201	2674	275944
2150	292	4141	13652	2347	269237
2160	541	5759	13319	3391	247593
2170	685	7661	13176	4384	202527
2180	798	7349	10689	5042	178633
2190	737	8154	10535	5273	189525
2200	847	9496	10605	6819	164266
2210	1180	12029	9974	8440	142997
2220	1237	13084	9637	8074	113632
2230	1071	10384	8964	6873	105959
2240	1289	13598	11104	8183	124531
2250	1355	14583	11322	9199	111636
2260	1002	10714	9733	7382	101713
2270	1008	11844	9589	7719	116853
2280	1478	14024	12658	9541	129399
2290	962	9417	12053	5315	85146
2300	25	190	-571	-622	578

10kV Data – Continued

Depth (mm)	Ti	V	Cr	Mn	Fe
10	646	208	88	201	9475
20	718	247	47	211	9324
30	574	83	123	360	8584
40	662	177	58	228	8179
50	743	91	46	375	8511
60	870	278	-3	269	10905
70	646	78	126	371	12122
80	470	168	17	243	13067
90	1065	120	175	398	14718
100	533	137	173	290	15843
110	1770	320	92	378	17780
120	1936	230	214	308	18731
130	601	254	112	361	13464
140	659	274	172	365	13259
150	434	160	198	298	12183
160	1512	204	211	409	13628
170	1776	330	191	564	15798
180	4084	305	127	501	34499
190	4710	388	-30	546	38251
200	3983	75	44	326	38517
210	2779	55	63	195	37451
220	2334	-30	118	-30	36597
230	2811	-98	127	96	40266
240	4319	210	89	344	38039
250	6233	408	86	562	41910
260	4450	355	51	382	40540
270	3485	257	248	172	35297
280	3163	265	120	227	33555
290	4144	185	65	204	45389
300	4313	34	-17	189	49518
310	4517	259	-35	412	44026
320	5001	506	6	437	42226
330	4583	403	130	604	41764
340	4604	425	35	385	42381
350	3896	52	-57	362	42851
360	4213	128	88	292	45000
370	3851	124	5	161	44303
380	3212	157	85	187	35397
390	3527	50	158	167	39339
400	4009	245	52	323	41164
410	5074	157	188	310	44169
420	4802	224	-1	365	45151

430	4930	377	50	405	45170
440	3442	149	165	305	35862
450	2578	95	118	163	29560
460	2038	3	326	313	28279
470	2391	-2	-25	164	32073
480	2527	222	147	137	29264
490	3221	342	191	279	26239
500	1236	-13	237	155	23139
510	2556	258	76	558	23291
520	2597	249	134	331	22438
530	1553	-81	85	191	23556
540	2035	26	51	156	26208
550	1764	249	209	265	18274
560	1956	141	153	344	21247
570	2224	281	139	276	17396
580	2701	343	146	335	27036
590	2448	359	102	297	24055
600	1864	-1	47	146	27547
610	1763	-34	124	197	19946
620	1429	108	57	221	17517
630	1209	139	123	320	13563
640	1400	152	97	286	18934
650	2218	84	163	239	21821
660	2446	142	98	263	23443
670	1565	164	122	167	13140
680	1978	158	7	313	16976
690	1994	115	50	129	21119
700	1312	60	103	360	16821
710	1071	73	111	424	13458
720	1000	150	23	185	15645
730	1503	68	197	365	16295
740	1366	113	149	301	11977
750	1443	343	104	418	12510
760	1550	285	127	313	13508
770	740	121	186	188	10866
780	783	223	145	165	13371
790	261	139	71	242	12351
800	1600	209	70	392	13421
810	763	101	33	230	11118
820	982	131	275	320	14612
830	1328	92	43	194	20598
840	575	109	93	269	9825
850	985	165	8	201	12493
860	1233	85	84	313	15814
870	613	96	40	612	10694
880	1831	96	103	404	20116
890	2384	266	34	347	22910
900	1903	128	41	529	20871
910	2408	368	147	425	24706

920	1922	58	196	223	28313
930	3298	99	-50	130	42116
940	1091	305	300	130	23763
950	1172	125	66	93	22447
960	2233	320	184	340	21366
970	1467	382	136	299	15427
980	3047	297	128	304	25618
990	1965	90	210	188	21715
1000	2503	-91	131	154	40051
1010	1375	151	169	167	23933
1020	1522	77	156	91	29010
1030	1506	135	320	346	19121
1040	2852	221	140	635	29729
1050	2978	322	105	414	28199
1060	1391	233	70	173	15398
1070	274	147	78	69	10368
1080	352	75	81	235	10115
1090	312	185	109	150	10415
1100	7	184	95	146	6636
1110	492	294	105	328	5767
1120	627	311	71	457	5494
1130	725	433	147	516	5217
1140	481	339	251	399	4849
1150	-231	202	152	91	4050
1160	-50	209	102	279	5130
1170	83	195	288	180	6171
1180	172	393	376	199	6353
1190	681	341	250	281	7109
1200	614	240	160	338	6851
1210	420	253	259	448	5514
1220	168	197	273	123	5337
1230	-22	168	315	147	5952
1240	164	195	141	131	6822
1250	549	184	244	198	8700
1260	648	175	210	206	9017
1270	832	166	205	264	10687
1280	856	263	217	296	10218
1290	1392	160	203	297	16080
1300	327	152	193	252	8506
1310	399	234	144	169	7666
1320	177	235	259	215	5015
1330	394	334	285	180	7787
1340	277	342	307	388	4709
1350	358	149	202	223	5320
1360	251	213	-21	217	2211
1370	98	98	-24	61	386
1380	79	134	110	144	4061
1390	3	306	388	146	4168
1400	797	391	140	247	15819

1410	172	211	344	187	4514
1420	315	295	310	212	4974
1430	293	288	255	385	5413
1440	368	301	218	317	5741
1450	243	296	269	283	5490
1460	10	409	123	176	5555
1470	158	305	156	224	6144
1480	480	144	148	204	8862
1490	2031	267	161	404	13589
1500	1249	176	87	286	8819
1510	901	305	127	325	7100
1520	293	155	130	251	4193
1530	-15	400	375	200	4206
1540	-45	435	432	222	4125
1550	52	250	341	226	4192
1560	161	336	247	409	3868
1570	347	294	251	404	3706
1580	220	245	243	332	3295
1590	313	459	428	393	3474
1600	38	397	253	86	3327
1610	67	410	396	372	3240
1620	10	178	145	203	3385
1630	72	226	153	266	3023
1640	325	274	145	387	3298
1650	348	335	174	443	3300
1660	299	238	51	470	3244
1670	160	267	87	358	2996
1680	282	237	114	248	3161
1690	22	243	40	237	2369
1700	519	372	67	361	3067
1710	253	263	111	478	2924
1720	154	284	206	294	2655
1730	46	222	265	275	2585
1740	159	276	204	335	2920
1750	32	333	323	349	2894
1760	66	338	223	257	2877
1770	272	357	97	399	2990
1780	429	256	104	306	3636
1790	355	319	178	311	3230
1800	250	140	130	329	3779
1810	28	244	378	341	4365
1820	14	346	294	253	4168
1830	-2	210	121	289	4243
1840	243	224	215	404	4620
1850	358	181	258	286	4950
1860	290	215	309	256	5636
1870	7	293	75	267	5840
1880	-123	252	239	58	5782
1890	37	170	138	197	6017

1900	272	230	5	234	5824
1910	645	224	178	312	5497
1920	486	268	169	218	7985
1930	426	369	321	256	7032
1940	666	166	46	251	7135
1950	552	229	201	274	6944
1960	122	101	117	255	8001
1970	-168	337	63	144	4833
1980	300	210	196	686	5394
1990	420	334	274	708	5720
2000	482	369	305	357	7132
2010	56	280	433	292	4647
2020	174	142	127	202	7203
2030	200	191	195	182	10267
2040	918	205	249	397	14422
2050	844	181	233	300	8917
2060	1558	262	114	407	16815
2070	1258	233	218	469	15230
2080	580	246	159	390	14042
2090	1287	283	158	382	18202
2100	2255	220	44	404	28664
2110	1764	95	114	488	21988
2120	882	287	19	462	6622
2130	791	229	138	548	6411
2140	661	248	281	667	6310
2150	69	243	-22	320	6431
2160	294	230	171	408	9239
2170	603	85	-20	321	13690
2180	1024	27	84	362	13946
2190	1778	222	59	361	13739
2200	2315	394	130	429	18063
2210	2777	324	85	319	24271
2220	2633	159	239	450	27425
2230	1884	22	100	254	23551
2240	2366	3	39	202	28447
2250	2942	341	244	495	30236
2260	2767	191	111	487	26931
2270	2700	294	91	356	25315
2280	3144	304	172	530	31491
2290	1911	88	131	248	25577
2300	111	50	46	15	122

30 kV Data

Depth (mm)	Zn	Br	Sr	Zr	Mo
10	216	1067	26658	2770	371
20	293	1470	26507	2398	154
30	288	1324	25365	2102	368
40	344	1182	24036	2148	331
50	213	1108	23517	2215	367
60	261	1245	23622	2453	204
70	227	880	23056	2695	448
80	259	1450	28074	3116	326
90	276	1289	26270	3292	355
100	360	1009	25358	3354	380
110	326	1327	24537	3245	505
120	441	1316	26273	3329	226
130	307	1200	27547	3016	341
140	301	1188	28136	3409	461
150	351	1274	27211	3270	551
160	331	1280	27412	3125	346
170	363	1374	25776	3219	607
180	463	1345	16885	3879	486
190	686	1344	19006	4373	675
200	621	1086	12099	3835	223
210	561	1172	11551	3795	554
220	568	1081	10763	3954	736
230	607	1150	11563	3906	637
240	466	953	10362	3315	548
250	567	1248	12028	4401	625
260	502	1052	10278	3879	415
270	443	1128	8930	3576	97
280	433	763	8747	3481	300
290	562	1160	11795	4407	320
300	584	1266	12861	4258	413
310	635	1171	13066	5091	816
320	631	1563	12405	4699	391
330	542	1014	11318	3507	460
340	597	945	11197	4003	390
350	536	1282	13377	4633	384
360	580	1133	13608	3886	611
370	586	1097	12322	4747	657
380	453	994	10095	3789	721
390	529	1235	11874	3741	880
400	551	1252	11869	4463	328
410	643	1128	13158	3963	555
420	615	1200	13946	4382	631

430	612	1262	14789	4442	607
440	596	1178	15893	4049	677
450	452	1180	18625	3440	428
460	482	1231	17154	3913	348
470	485	1008	13966	4248	477
480	509	1100	14360	3644	732
490	389	873	13059	3051	716
500	383	942	14778	3488	450
510	363	1019	13907	3092	482
520	429	867	11836	2764	398
530	364	960	11640	2900	176
540	381	1115	12501	3393	248
550	242	760	11191	2405	343
560	339	832	16122	3073	532
570	393	865	17491	3333	427
580	391	979	13790	3544	324
590	341	1050	13878	3057	657
600	400	1059	13351	2740	118
610	305	1027	14894	2901	490
620	380	1022	14450	2594	418
630	310	981	17332	2420	294
640	260	851	18675	3520	236
650	457	859	20540	3330	419
660	319	966	12865	2945	278
670	285	767	12100	2000	327
680	363	692	12976	2978	325
690	374	932	14031	2820	264
700	375	1114	23515	3378	271
710	274	889	17117	2821	399
720	223	763	14311	2570	475
730	251	820	13408	2398	397
740	219	813	14791	2322	583
750	286	988	16985	2404	414
760	203	917	20145	2596	1024
770	223	943	21199	2814	320
780	235	1128	22835	3134	442
790	310	1064	24352	2767	681
800	239	975	23325	2989	665
810	177	655	17362	2521	285
820	215	1052	23501	3157	622
830	241	738	16019	2895	517
840	164	797	16802	2852	366
850	212	857	15572	2564	387
860	246	849	13889	2967	239
870	279	1128	23287	2620	405
880	337	1085	22641	3415	433
890	317	946	15793	2796	312
900	426	1224	22405	3413	246
910	348	1072	18842	3784	335

920	518	850	12581	4102	684
930	378	1106	19211	3212	407
940	293	1162	18387	3213	359
950	348	1070	16903	2887	294
960	276	935	24534	3434	245
970	522	1338	19931	3702	591
980	377	950	21121	3738	361
990	476	971	14799	4695	551
1000	351	1080	21421	4001	270
1010	404	911	20938	3559	743
1020	292	854	22735	3304	394
1030	422	1019	17936	4765	532
1040	350	1042	19470	3328	805
1050	310	867	23360	3249	612
1060	169	979	26786	2936	574
1070	204	1038	27775	4209	780
1080	202	988	29210	2788	429
1090	137	953	28056	2614	284
1100	203	1179	28311	2320	245
1110	157	945	29323	2578	227
1120	213	1087	29220	2284	451
1130	120	1084	30068	2397	440
1140	191	1314	31227	2403	570
1150	206	1184	31892	2667	652
1160	213	963	30892	3007	269
1170	142	1011	31304	2952	405
1180	154	1219	30397	2526	462
1190	172	918	29602	3053	481
1200	154	1107	30421	2471	603
1210	149	988	33444	2947	623
1220	207	1000	30113	2756	430
1230	176	952	26499	2136	530
1240	237	1051	29316	2978	320
1250	258	1130	28733	3249	326
1260	200	957	28474	2754	482
1270	151	1255	29809	2998	267
1280	330	1094	25757	3506	406
1290	206	1020	28528	2804	473
1300	184	1009	31616	2338	722
1310	157	1039	30886	2193	276
1320	171	1227	28314	2875	280
1330	119	1014	31782	2484	373
1340	210	1123	31761	2356	341
1350	95	728	7662	823	251
1360	72	313	1491	410	294
1370	171	1201	25128	2673	314
1380	165	1113	32852	2846	252
1390	342	1396	25633	3649	719
1400	114	1226	33217	2509	471

1410	165	1037	32515	2999	392
1420	176	1118	32725	2681	276
1430	173	1065	32655	2961	615
1440	132	1139	32640	2946	186
1450	136	1310	33128	2761	600
1460	173	1300	33057	2608	661
1470	227	1592	31102	2383	356
1480	298	1806	27502	2115	257
1490	183	1266	16371	1938	478
1500	156	1206	26450	2094	327
1510	213	1185	28402	2353	290
1520	195	1237	32777	2862	765
1530	167	1265	33599	2924	386
1540	125	848	33968	3045	363
1550	150	1041	31387	2407	361
1560	119	1041	30551	2501	258
1570	125	1000	29512	2451	526
1580	111	1134	31938	2614	278
1590	117	1057	32821	2420	351
1600	80	1104	30544	2092	608
1610	181	1252	33047	2460	506
1620	136	1048	32598	2549	285
1630	130	1064	30577	2307	465
1640	147	988	29979	2217	374
1650	153	1190	29862	2072	424
1660	177	998	29657	1856	357
1670	115	1102	29919	1928	609
1680	110	1063	29364	1868	709
1690	195	1106	29942	2086	561
1700	150	1131	30127	2145	266
1710	136	1000	32319	2084	340
1720	82	997	32627	2504	413
1730	206	1037	33276	2406	775
1740	120	1065	32974	2395	311
1750	212	1030	34384	2255	652
1760	201	998	30461	2394	250
1770	165	1040	27650	2295	493
1780	167	974	28091	2004	384
1790	179	914	31308	2583	314
1800	173	1066	33414	2577	388
1810	153	903	32538	2528	476
1820	131	978	32297	2493	302
1830	161	924	31590	2501	584
1840	181	968	30764	2499	530
1850	212	1060	31540	2742	566
1860	164	1057	29551	2611	656
1870	151	1146	30213	2822	434
1880	176	1175	30993	2435	788
1890	180	937	22308	2216	521

1900	141	891	22045	1901	387
1910	160	1147	28666	2935	225
1920	112	1035	28103	2793	335
1930	189	967	24017	2458	365
1940	166	1072	24452	2705	668
1950	229	1043	25714	2426	192
1960	105	927	26740	2462	290
1970	170	756	26445	2134	318
1980	248	1068	29557	2616	333
1990	162	1157	28718	2562	306
2000	117	1136	30164	2892	399
2010	176	1256	29072	3082	395
2020	271	1104	28545	3236	516
2030	358	1222	27319	3302	369
2040	300	1293	27625	2843	355
2050	355	1312	21440	3439	432
2060	325	1183	23865	3455	370
2070	338	1248	25218	2865	390
2080	406	1354	23372	3521	939
2090	486	1219	17188	3847	621
2100	408	1195	17721	3188	422
2110	246	987	22887	2435	315
2120	238	1041	24577	1989	237
2130	203	1153	25690	2328	389
2140	205	1110	26767	2332	348
2150	187	1171	24291	2868	477
2160	297	1337	21540	2994	534
2170	262	1048	18782	2856	324
2180	299	1032	19449	2781	423
2190	400	1092	17917	3306	329
2200	452	1188	14243	3801	311
2210	492	1131	13955	3504	199
2220	299	981	13197	2733	307
2230	383	902	15043	4246	469
2240	402	1097	13649	4078	331
2250	366	892	11906	2989	488
2260	394	942	12993	2780	605
2270	489	1256	15532	3757	417
2280	380	1267	9482	2562	395
2290	38	64	101	105	151

50 kV Data

Depth (mm)	Ba
10	436
20	527
30	495
40	470
50	495
60	577
70	727
80	611
90	584
100	775
110	700
120	820
130	600
140	686
150	675
160	683
170	593
180	745
190	628
200	556
210	604
220	311
230	682
240	585
250	696
260	625
270	546
280	681
290	717
300	741
310	730
320	790
330	533
340	735
350	828
360	886
370	693
380	655
390	739
400	682
410	674
420	696
430	772
440	603

450	649
460	624
470	561
480	711
490	511
500	536
510	433
520	338
530	576
540	403
550	221
560	479
570	496
580	524
590	580
600	411
610	500
620	577
630	396
640	546
650	532
660	513
670	222
680	350
690	420
700	432
710	439
720	400
730	334
740	405
750	490
760	569
770	486
780	471
790	614
800	187
810	571
820	550
830	414
840	352
850	358
860	327
870	692
880	586
890	491
900	496
910	476
920	468
930	619

940	596
950	516
960	590
970	642
980	646
990	853
1000	682
1010	666
1020	746
1030	512
1040	550
1050	596
1060	477
1070	285
1080	433
1090	402
1100	445
1110	334
1120	408
1130	430
1140	393
1150	327
1160	450
1170	433
1180	395
1190	425
1200	584
1210	475
1220	581
1230	536
1240	407
1250	432
1260	491
1270	608
1280	611
1290	392
1300	548
1310	423
1320	514
1330	509
1340	552
1350	406
1360	247
1370	88
1380	468
1390	437
1400	753
1410	411
1420	493

1430	464
1440	506
1450	517
1460	434
1470	443
1480	428
1490	333
1500	308
1510	332
1520	429
1530	440
1540	365
1550	395
1560	450
1570	553
1580	495
1590	489
1600	567
1610	575
1620	600
1630	617
1640	408
1650	333
1660	339
1670	415
1680	473
1690	397
1700	304
1710	410
1720	357
1730	410
1740	428
1750	405
1760	334
1770	369
1780	245
1790	357
1800	299
1810	354
1820	311
1830	385
1840	482
1850	426
1860	466
1870	438
1880	444
1890	408
1900	394
1910	435

1920	563
1930	591
1940	385
1950	419
1960	555
1970	634
1980	548
1990	574
2000	617
2010	622
2020	627
2030	691
2040	753
2050	769
2060	937
2070	914
2080	775
2090	1084
2100	1008
2110	893
2120	600
2130	426
2140	459
2150	483
2160	620
2170	773
2180	559
2190	632
2200	804
2210	612
2220	574
2230	534
2240	533
2250	538
2260	457
2270	396
2280	442
2290	360
2300	23

APPENDIX D: Calibration plots for EWR 2010 radiocarbon results. Figures from www.http://radiocarbon.ldeo.columbia.edu/research/radcarbcal.htm Top plot 150mm - Bottom plot 810mm

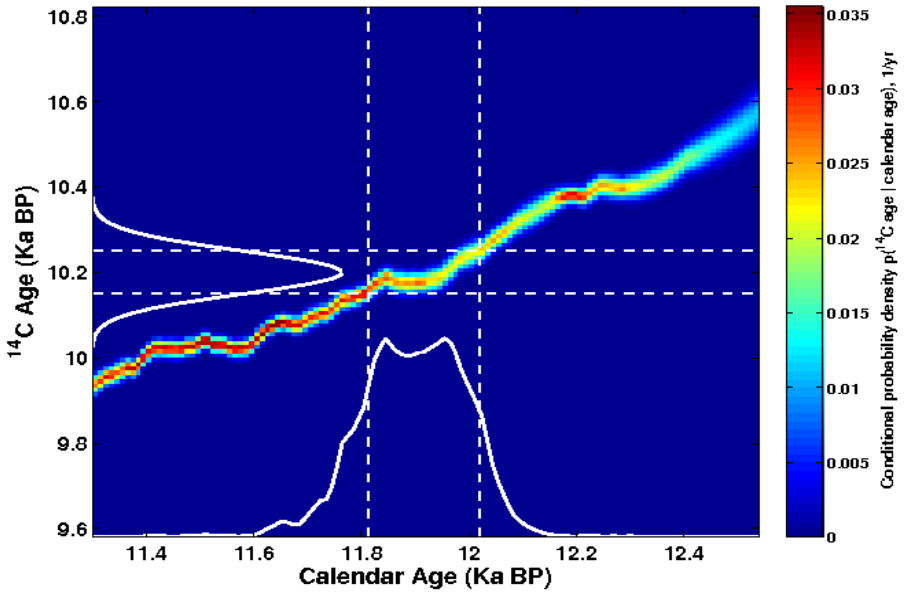

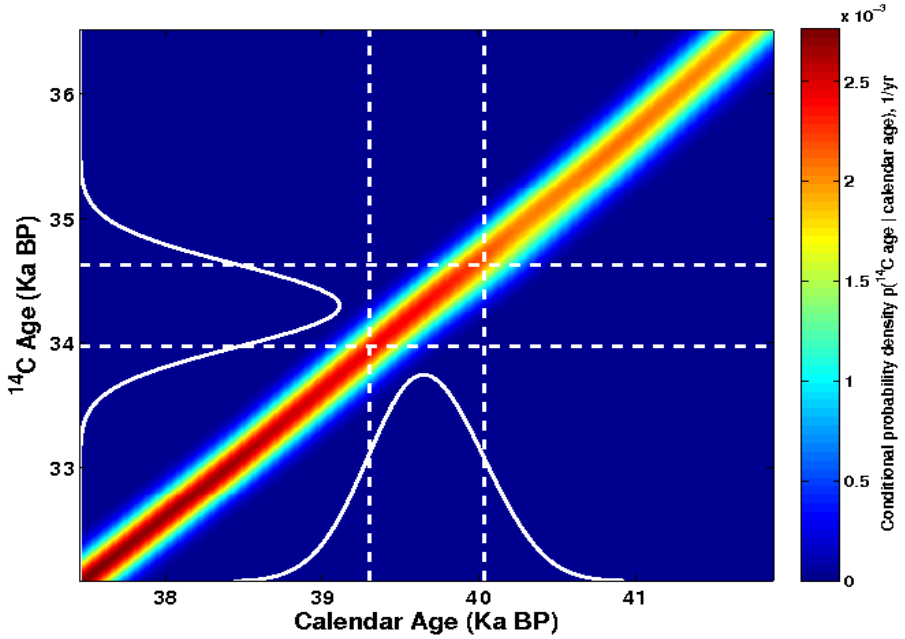

References

Alley R.B.; Marotzke J.; Nordhaus W.D.; Overpeck J.T.; Peteet D.M.; Pielke R.A. Jr.; Pierrehumbert R.T.; Rhines P.B.; Stocker T.F.; Talley L.D.; Wallace J.M. (2003) Abrupt Climate Change, *Science*, 299, 2005-2010

Arthur, M.A. and Sageman, B.B. (1994) Marine black shales: a review of depositional mechanisms and environments of ancient deposits, *Annual Review of Earth and Planetary Science*, 22, 499-552

Arthur, M.A., Dean, W.W, Pollastro, R., Scholle, P.A., Claypool, G.E. (1985) A comparative geochemical study of two transgressive pelagic limestone units, Cretaceous Western Interior Basin, U.S. in Fine-grained deposits and biofacies of the Cretaceous Western Interior Seaway: evidence of cyclic sedimentary processes. Eds. L.M. Pratt, E.G. Kauffman and F.B. Zelt, *Society of Economic Paleontologists and Mineralogists*, Tulsa, OK, 16-27

Baes, C.I. and Mesmer, R.E. (1976) The hydrolysis of cations. New York, John Wiley

Balsam, W.L. (1981) Late Quaternary sedimentation in the western North Atlantic: Stratigraphy and paleoceanography, *Paleogeography, Paleoclimatology and Paleoecology*, 35, 215-240

Balsam, W.L. and Heusser, L.E. (1976) Direct correlation of sea surface paleotemperatures, deep circulation, and terrestrial paleoclimates: Foraminiferal and palynological evidence from two cores off Chesapeake Bay, *Marine Geology*, 21, 121-147

Balsam, W.L. and McCoy, F.W. Jr. (1987) Atlantic Sediments: Glacial/Interglacial Comparisions, *Paleoceanography*, 2, 531-542

Berger, W.H. (1982) Increase of carbon dioxide in the atmosphere during deglaciation: The coral reef hypothesis, *Naturwissenschaften*, 69, 87-88

Berger, W.H. and Killingley, J.S. (1982) The Worthington Effect and the origin of the Younger Dryas, *Journal of Marine Research*, 40, 27-38

Berner, R.A. (1984) Sedimentary pyrite formation – an update, *Geochim. Cosmochim Acta*, 48, 605-615

Bond, G., Kromer, B., Beer, J., Muscheler, R., Evans, M.N., Showers, W., Hoffman, S., Lotti-Bond, R., Hajdas, I., Bonani, G. (2001) Persistent solar influence on North Atlantic climate during the Holocene, *Science*, 294, 2130-2136

Bond, G. and Lotti, R. (1995) Iceberg discharges into the North Atlantic on millennial time scales during the last glaciation, *Science*, 267, 1005-1010

Broecker, W.S. (1982) Ocean geochemistry during glacial time, *Geochim. Cosmochim. Acta*, 46, 1689-1705

Broecker, W.S. (1998) Paleocean Circulation during the last deglaciation: a bipolar seesaw? *Paleoceanography*, 13, 119-121

Brovkin, V., Ganopolski, A., Archer, D., Rahmstorf, S. (2007) Lowering of glacial atmospheric CO_2 in response to changes in oceanic circulation and marine biogeochemistry, *Paleoceanography*, 22

Burdige, D.J. (2006) Geochemistry of Marine Sediments, Princeton, Woodstock, Princeton University Press

Canfield, D.E., Riaswell, R., Bottrell, S. (1992) The reactivity of sedimentary iron minerals toward sulfide, *Amer. Journal Sci*, 292, 659-683

Clark, P.U., Alley, R.B., Pollard, D. (1999) Northern hemisphere ice-sheet influences on global climate change, *Science*, 286, 1104-1111

Dansgaard, W., Johnsen, S.J., Clausen, H.B., Dahl-Jensen, D., Gundestrup, N.S., Hammer, C.U., Hvidberg, C.S., Steffensen, J.P., Sveinbjörnsdottir, A.E., Jouzel, J., Bond, G. (2003) Evidence for general instability of past climate from a 250k-year ice-core record, *Nature*, 364, 218-220

Emiliani, C., (1955). Pleistocene temperatures. *Journal of Geology*, 63, 538– 578.

Fairbanks, R.G., Mortlocka, R.A., Chiua, T., Caoa, L., Kaplana, A., Guildersonc, T.P., Fairbanks, T.W., Bloomf, A.L., Grootes, P.M., Nadeaug, M. (2003) Radiocarbon calibration curve spanning 0 to 50,000 years BP based on paired 230Th/ 234U/ 238U and 14C dates on pristine corals, *Quaternary Science Reviews*, 24, 1781-1796

Froelich, P.N., Klinkhammer, G.P., Bender, M.L., Luedtke, N.A., Heath, G.R., Cullen, D., Dauphin, P., Hammond, D., Hartman, B., Maynard, V. (1978) Early oxidation of organic matter in pelagic sediments of the eastern equatorial Atlantic: suboxic diagenesis, *Geochim. Cosmochim. Acta*, 43, 1075-1090

Ganachaud, A. and Wunsch, C. (2000) Improved estimates of global ocean circulation, heat transport and mixing from hydrographic data, *Nature*, 408, 453-457

Ganapolski, A. and Rahmstorf, S. (2000) A possible mechanism for Dansgaard-Oeschger events, *Geophysical Research Abstracts*, 2

Goldhaber, M.B. and Kaplan, I.R. (1974) The sulfur cycle. In Goldberg, E.D., The Sea; New York, Wiley, 569-655

Gorsline, D.S. (1984) A review of fine-grained sediment origins, characteristics, transport and deposition. In Fine-grained sediments: Deep-water processes and facies, *Geological Society of America Special Publications*, eds. D.A.V. Stow and D.J.W. Piper, Geological Society of America, Boulder, CO, 17-34

Hays, J.D., Imbrie, J., Shackleton, N.J. (1976) Variations in the Earth's orbit; pacemaker of the ice ages, *Science*, 194, 1121-1132

Jaccard, S.L., Haug, G.H., Sigman, D.M., Pedersen, T.F., Thierstein, H.R., Röhl, U. (2005) Glacial/Interglacial changes in subarctic North Pacific stratification, *Science*, 308, 1003-1006

Jorgensen, B.B. (1977) Bacterial sulfate reduction within marine microniches of oxidized marine sediments, *Marine Biology*, 41, 7-17

Jouzel, J., Masson-Delmotte, V., Cattani, O., Dreyfus, G., Falourd, S., Hoffmann, G., Minster, B., Nouet, J., Barnola, J.M., Chapellaz, H., Fischer, J.C., Gallet, S., Johnsen, M., Leuenberger, L., Loulergue, D., Luethi, H., Oeter, F., Parrenin, G., Raisbeck, D., Raynaud, A., Schilt, J., Schwander, E., Selmo, R., Souchez, R., Spahni, B., Stauffer, J.P., Steffensen, B., Stenni, T.F., Stocker, J.L., Tilson, M., Werner, E., Wolf, W. (2007) Orbital and millennial Antarctic climate variability over the past 800,000 years, *Sceince*, 317, 793-797

Keigwin, L.D. and Jones, G.A. (1994) Western North Atlantic evidence for millennial-scale changes in ocean circulation and climate, *Journal of Geophysical Research*, 99, 12,397-12,410

Krom, M.D. and Berner, R. A. (1980) Adsorption of phosphate in anoxic marine sediments, *Limnology and Oceanography*, 5, 797-806

Kuypers, M.M., Blokker, P., Erbacher, J., Kinkel, H., Pancost, R.D., Schouten, S., Sinninghe, D., Jaap S. (2001) Massive expansion of marine Archaea during a Mid-Cretaceous oceanic anoxic event, *Science*, 293, 92-94

Lisiecki, L.E. and M.E. Raymo. (2005) A Pliocene-Pleistocene stack of 57 globally distributed benthic D18O records, *Paleoceanography*, 20

Lynch-Stieglitz, J., Adkins, J.F., Curry, W.B. (2007) Atlantic meridional overturning calculation during the Last Glacial Maximum, *Science*, 316, 66-69

Mayer, L.M., Macko, S.A., Mook, W.H., Murray, S. (1981) The distribution of bromine in coastal sediments and its use as a source indicator for organic matter, *Organic Geochemistry*, 3, 37-42

Nederbragt, A.J., Thurow, J., Vonhof, H., Brumsack, H.J., (2004) Modelling oceanic carbon and phosphorus fluxes; implications for the cause of the late Cenomanian Oceanic Anoxic Event (OAE2), *Jour. Geological Society London*, 161, 721-728

Paillard, D., Labeyrie, L., Yioy, P. (1996) Macintosh program performs time-series analysis, *Eos transactions, AGU*, 77, 379

Paytan, A. and Kastner, M. (1996) Benthic Ba fluxes in the central Equatorial Pacific, implications for the oceanic Ba cycle, *Earth and Planetary Science Letters*, 142, 439-450

Potter, P.E., Maynard, B.J, Pryor, W.A. (1980) Sedimentology of shale: Study guide and reference source, Springer, New York, 270pp.

Pratt, L.M. (1984) Influence of paleoenvironmental factors on preservation of organic matter in the middle Cretaceous Green Formation, Pueblo, CO, *American Association of Petroleum Geology Bulletin*. 68, 1146-1159

R Development Core Team (2010) R: A language and environment for statistical computing, Vienna, Austria. ISBN 3-900051-00-3, <http://www.Rproject.org>

Redfield, A.C., (1934) On the proportions of organic derivations and their relation to the composition of plankton, *James Johnston Memorial Volume*, University Press of Liverpool, 177-192

Richard, F.C. and Bourg, A.C.M. (1991) Aqueous geochemistry of chromium: a review, *Water Research*, 25, 807-816

Ruddiman, W.L. and Bowles, F.A. (1976) Early interglacial bottom-current sedimentation on the eastern Reykjanes Ridge, *Marine Geology*, 21, 191-210
Ruddiman W.F. and McIntyre, A. (1981) Oceanic mechanism for amplification of the 23,000 year ice-volume cycle, *Science*, 212, 617-627

Ruddiman, W.F. and McIntyre, A. (1984) Ice-age thermal response and climatic role of the surface North Atlantic Ocean, 40° to 63°N, *Geological Society of America Bulletin*, 95, 381-396

Ruddiman, W.F., M . E. Raymo, M.E., Martinson, D.G., Clement, B.M., Backman, J. (1989) Pleistocene Evolution: Northern Hemisphere ice sheets and North Atlantic Ocean, *Paleoceanography*, 4, 353-412

Ruttenberg, K.C. (1992) Development of a sequential extraction method for different forms of phosphorous in marine sediments, *Limnol. Oceanogr.*, 37, 1460-1482

Ruttenberg, K.C. (1993) Reassessment of the oceanic residence time of phosphorous, *Chemical Geology*, 107, 405-409

Schmitz, B. (1987) Barium, equatorial high productivity and the wandering of the Indian Continent, *Paleoceanography*, 2, 63-77

Seigenthaler, U., Stocker, T.F., Monnin, E., Luthi, D., Schwander, J., Staufer, B., Raynaud, D., Barnola, J.M., Fischer, H., Masson-Delmotte, V., Jouzel, J. (2005) Stable carbon cycle-climate relationship during the late Pleistocene, *Science*, 310, 1313-1317

Schimmield, G.B., Price, N.B., Kahn, A.A. (1988) The use of Th-230 and Ba as indicators of paleoproductivity over a 300Kyr time scale – Evidence from the Arabian Sea, *Chemical Geology*, 70, 112

Slopm, C.P., Van Der Gaast, S.J., Van Raaphorst, W. (1996) Phosphorous Binding by Poorly Crystalline Iron Oxides in North Sea Sediments, *Maine Chemistry*, 52, 55-73

Tamburini, F. (2001) Phosphorous in marine sediments during the last 150,000 years: exploring relationships between continental weathering, productivity, and climate, Unpublished doctoral dissertation, Université de Neuchâtel

Tamburini, F., Huon, S., Steinmann, P., Grousset, F.E., Adatte, T., Follmi, K. (2002) Dysaerobic conditions during Heinrich events 4 and 5: evidence from phosphorous distribution in a North Atlantic deep-sea core, *Geochim. Cosmochim. Acta*, 66, 4069-4083

Tamburini, F., Adatte, T., Follmi, K., Bernasconi, S.M., Steinmann, P. (2003a) Investigating the history of East Asian monsoon and climate during the last glacial-interglacial period (0-140,000 years): mineralogy and geochemistry of ODP sites 1143 and 1144, South China Sea, *Marine Geology*, 201, 147-168

Tabmurini, F., Follmi, K., Adatte, T., Bernasconi, S.M., Steinmann, P. (2003b) Sedimentary phosphorous records from the Oman margin: New evidence for high productivity during glacial periods, *Paleoceanography*, 18, 15-1 – 15-14

Thunell, R.C. (1982) Carbonate dissolution and abyssal hydrography in the Atlanic Ocean, *Marine Geology*, 47, 165-180

Tortell, P.D., Maldonado, M.T., Price, N.M. (1996) The role of heterotrophic bacteria in iron-limited ecosystems, *Nature*, 383, 330-332

Wehrli, B. and Stumm, W. (1989) Vanadyl in natural waters: Adsorbtion and hydrolysis promote oxygenation, *Geochim. Cosmochim. Acta*, 53, 69-77
Ziegler, M., Jilbert,T., de Lange, G.J., Lourens, L.J., and Reichart, G.-J., 2008, Bromine counts from XRF scanning as an estimate of the marine organic carbon content of sediment cores, *Geochemistry, Geophysics, Geosystems*, 9, Q05009, doi:10.1029/2007GC001932.